POLITECNICO
MILANO 1863

SCUOLA DI INGEGNERIA INDUSTRIALE
E DELL'INFORMAZIONE

Design of a Cherenkov detector for very-high-energy gamma rays

Tesi di Laurea Magistrale in
Space Engineering - Ingegneria Spaziale

Author: **Sofia Grusovin**

Student ID: 940015
Advisor: Prof. Giovanni Consolati

Academic Year: 2021-22

Abstract

Context. An international collaboration is working on the realization of a next-generation observatory situated in the Southern hemisphere, which offers a privileged view on the center of the galaxy: the Southern Wide-field Gamma-ray Observatory (SWGO).
Aims. The Italian partners of the SWGO collaboration (Istituto Nazionale di Fisica Nucleare (INFN), Politecnico di Milano and the universities of Torino, Padova and Napoli) are working on the construction of a prototype water Cherenkov detector in Politecnico di Milano, to use as a flexible testing facility.
Methods. An analytical study on muons' showers (the only particles detectable at Milano's altitude) has been carried out with the use of the HAWCSim software to study the correlation between the detection capabilities of the prototype tank and the water level with the purpose of choosing the water level for the tests and consequently an installation site that could handle the pressure. At the same time, a structure able to hold different types of detectors in multiple configurations has been designed: first a CAD model in SolidWorks has been realized for load simulations and then the structure has been built and tested in Politecnico's labs.
Results. The simulations showed a linear increase of detection efficiency with the water level, as well as an increase of the number of photoelectrons (PE) detected and a reduction of the dispersion of the detection time of the first photon. The photomultipliers holder has been designed in two versions: a large hexagonal one capable of handling a high number of sensors configurations and a small cross-shaped one, more simple and economic, for starting the tests with the reference configuration. The second structure has been built and tested; its pieces will be recycled for the larger one afterwards. As soon as the tank construction is completed, the first tests will start.

Keywords: very-high-energy gamma rays; Cherenkov detector; ground-based; photomultiplier tubes; Extensive Air Showers; SWGO

Abstract in lingua italiana

Contesto. Una collaborazione internazionale sta lavorando alla realizzazione di un osservatorio di nuova generazione situato nell'emisfero Sud, che offre una vista privilegiata sul centro della galassia: il Southern Wide-field Gamma-ray Observatory (SWGO).
Obiettivi. I partner italiani della collaborazione SWGO (Istituto Nazionale di Fisica Nucleare(INFN), il Politecnico di Milano e le università di Torino, Padova e Napoli) stanno lavorando alla costruzione di un prototipo di rilevatore Cherenkov ad acqua al Politecnico di Milano, da usare come struttura di test.
Metodi. Uno studio analitico su sciami di muoni (le uniche particelle rilevabili all'altitudine di Milano) è stato fatto con l'uso del software HAWCSim per studiare la correlazione tra le capacità di rilevazione della tank prototipo ed il livello dell'acqua, allo scopo di scegliere il livello dell'acqua per gli esperimenti e conseguentemente un sito di installazione che potesse sostenere la pressione. Contemporaneamente, è stata progettata una struttura in grado di sostenere diversi tipi di sensori in varie configurazioni: prima è stato realizzato un modello CAD in SolidWorks per le simulazioni di carico e poi la struttura è stata costruita e testata nei laboratori del Politecnico.
Risultati. Le simulazioni hanno mostrato un incremento lineare dell'efficienza di rilevazione con l'aumento del livello dell'acqua, un incremento nel numero di fotoelettroni rilevati e una riduzione della dispersione del tempo di rilevamento del primo fotone. La struttura per sostenere i fotomoltiplicatori è stata progettata in due versioni: una grande esagonale in grado di reggere un alto numero di configurazioni di sensori e una piccola a forma di croce, più semplice ed economica, per iniziare i test con la configurazione di riferimento. La seconda struttura è stata costruita e testata; i pezzi verranno poi riciclati per la struttura più grande. Appena la costruzione della tank sarà ultimata, inizieranno i primi esperimenti.

Parole chiave: raggi gamma ad altissima energia; rilevatore Cherenkov; ground-based; fotomoltiplicatori, Extensive Air Showers; SWGO

Contents

Introduction

0.1. Very-high-energy gamma rays

In the last decade there has been an important development of multi-messenger astronomy: the coordinated observation and interpretation of information from photons, cosmic rays, neutrinos and gravitational waves. This technique enabled the extension of the energy window through which the universe is observed, and consequently the variety of phenomena that can be studied.[37, 41] In this context, very-high-energy (VHE) gamma rays (from $100\ GeV$ to $100\ TeV$) are an element of particular interest for research. VHE gamma rays carry information from extreme astrophysical objects and phenomena such as neutron stars, black holes, supernova remnants and gamma-ray bursts. The study of VHE gamma rays could also provide answers to the many questions about the origin and acceleration of cosmic rays. Furthermore, extremely energetic photons can give information about the extragalactic background light, the quantum gravity effect and dark matter.[5, 13, 26]

Due to the declining flux emitted by cosmic sources (the flux of gamma rays from all sources drops rapidly as a function of energy), photons in this energy range can not be studied with direct measurements, therefore they are detected indirectly from ground-based instruments, by observing the particle cascades they produce in the atmosphere: the so-called extensive air showers (EASs). In gamma ray astronomy, two types of instruments are used to observe VHE photons: imaging atmospheric Cherenkov telescopes (IACT), which detect the light produced by the shower particles as they traverse atmosphere, and ground extensive air showers (EAS) detectors, which directly detect the shower particles at ground level (fig. 1). IACT detectors have better energy and position resolution and stronger background suppression, but their field of view is small ($< 10°$) and their duty cycle is low ($\sim 10 - 15\%$). EAS on the other hand have a high duty cycle (up to 100%) and a large field of view (~ 3 steradiants) but their angular and energy resolutions are limited, as their background discrimination. It is clear that the strengths and weaknesses of these two types of detectors are complementary and therefore the observation of the same phenomenon with both techniques is often useful.[5, 28, 43]

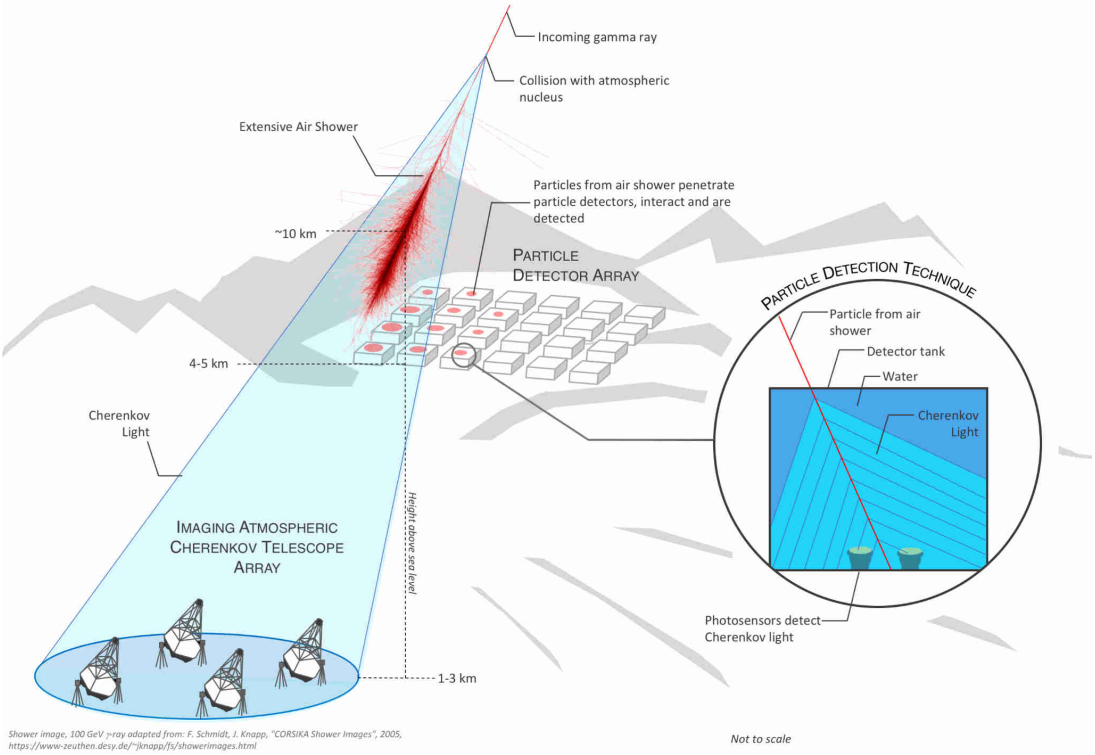

Figure 1: Schematic view of the IACT and EAS arrays detection techniques.[26]

0.2. State of the art

Until recently, IACTs dominated the field of ground-based gamma-ray astronomy with three major facilities providing coverage of both hemispheres: H.E.S.S., MAGIC and VERITAS.[5] EAS detectors were typically composed by sparse arrays of scintillation detectors distributed over large areas at moderate altitudes. The EAS particles reaching the ground are a lot fewer with respect to the photons that they generate by interacting with the atmosphere and, in addition to that, at low altitude, most of the shower particles have already been absorbed by the atmosphere. As a result, these sparse arrays typically sampled only a small fraction of the shower particles.[42]

In 1999, Milagro EAS observatory started operating (and remained operative until 2008). For this observatory, water Cherenkov technology was implemented. In a water detector, the EAS particles generate Cherenkov light by moving in the water at relativistic speed, providing an amplification effect and therefore making the particle detectable also by photomultiplier tubes (PMTs) that do not intersect their trajectory.[33, 42] (More on water Cherenkov detectors (WCDs) in section 0.3.1) The observatory was placed at 2630 m altitude, in the Jemez mountains in Nex Mexico. It was composed by a central 60 m x 80 m pond completed by a sparse 200 m x 200 m outrigger array ,made of 175 water

tanks. Its large field of view (2 steradiands) and high duty cycle (>90%) allowed Milagro to be the first EAS array capable of continuously monitoring the overhead sky for sources of TeV gamma rays and to discover new sources in that energy range.[12, 15, 30] IACTs, having a small field of view, can not study emission regions with large angular size, so the successes of Milagro proved the importance of investing in EAS detectors.

0.2.1. HAWC

After Milagro's success in fact, another observatory was built as a follow up experiment: the High Altitude Water Cherenkov gamma-ray observatory (HAWC), which started operating in 2015. HAWC is a gamma-ray and cosmic ray observatory located inside the Parque Nacional Pico de Orizaba in Mexico, at 4100 m altitude (significantly higher than Milagro). Instead of a single large pool, as Milagro, this observatory is composed by 300 water Cherenkov detectors with 3 peripheral and 1 central photomultiplier tube (PMT) each (fig. 2). This geometry provides better hadronic rejection due to optical isolation between the modules and a more precise reconstruction.[20, 30, 35] As mentioned before, the high altitude is a key factor for this kind of observatories since, the higher the altitude, the less particles have already been absorbed by the atmosphere. In addition to the altitude advantage, HAWC has a muon detection area an order of magnitude higher than Milagro's. These characteristics made it the first competitive instrument based on the EAS technique.[5, 18]

(a) Picture of the HAWC detector.[47]

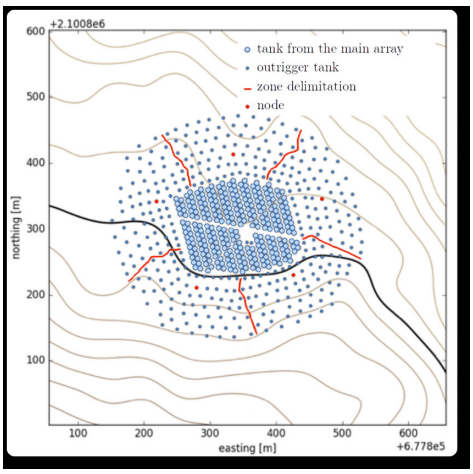

(b) Scheme of the HAWC detector's layout.[44]

Figure 2: The HAWC detector.

0.2.2. LHAASO

In 2019, the Large High Altitude Air Shower Observatory (LHAASO) started operating. It is a gamma ray and cosmic ray observatory located in Daocheng (Sichuan Province, China) at an altitude of 4410 m.[4, 31, 44] LHAASO is composed by three parts:

1. the Water Cherenkov Detector Array (WCDA), located at the center of the array, for surveying transient phenomena and discovering new sources
2. the Kilometer Square Array (KM2A), EAS detector made by 5195 scintillator counters and 1188 muon detectors
3. the Wide Field-of-view Cherenkov Telescope Array (WFCTA), counting 18 telescopes

covering together a range from 0.1 TeV to 1 PeV. The WCDA covers a 78000 m^2 area with closely packed water tanks, similar to the HAWC configuration but two times larger (fig. 3).[3, 4]

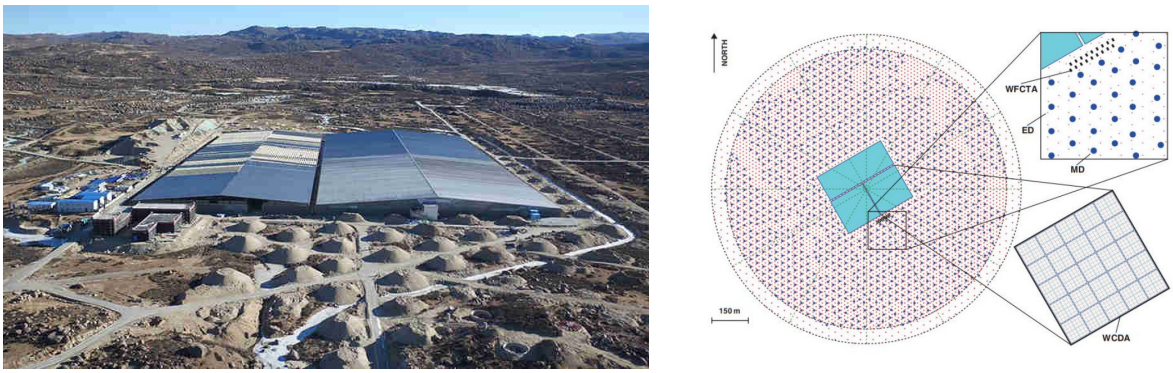

(a) Picture of the LHAASO.[47] (b) Scheme of LHAASO's layout.[44]

Figure 3: The LHAASO detector.

0.3. SWGO

Both HAWC and LHAASO have achieved very important results in the field of gammma rays and cosmic rays research, but both facilities are situated in the Northern hemisphere.

The Southern hemisphere has a privileged view of the galactic center (GC) region, where most galactic accelerators and astrophysical sources in general are located, therefore a detector placed in the Southern hemisphere would be an important tool for research and its observations would complement the ones of HAWC and LHAASO (fig. 4).[5, 26]

An international Southern Wide-field Gamma-ray Observatory (SWGO) collaboration has therefore formed to develop the plans for a ground-level particle detection based observatory, aiming for a performance at VHE comparable to that of LHAASO, and possibly better in the $\sim 100\ GeV$ region.

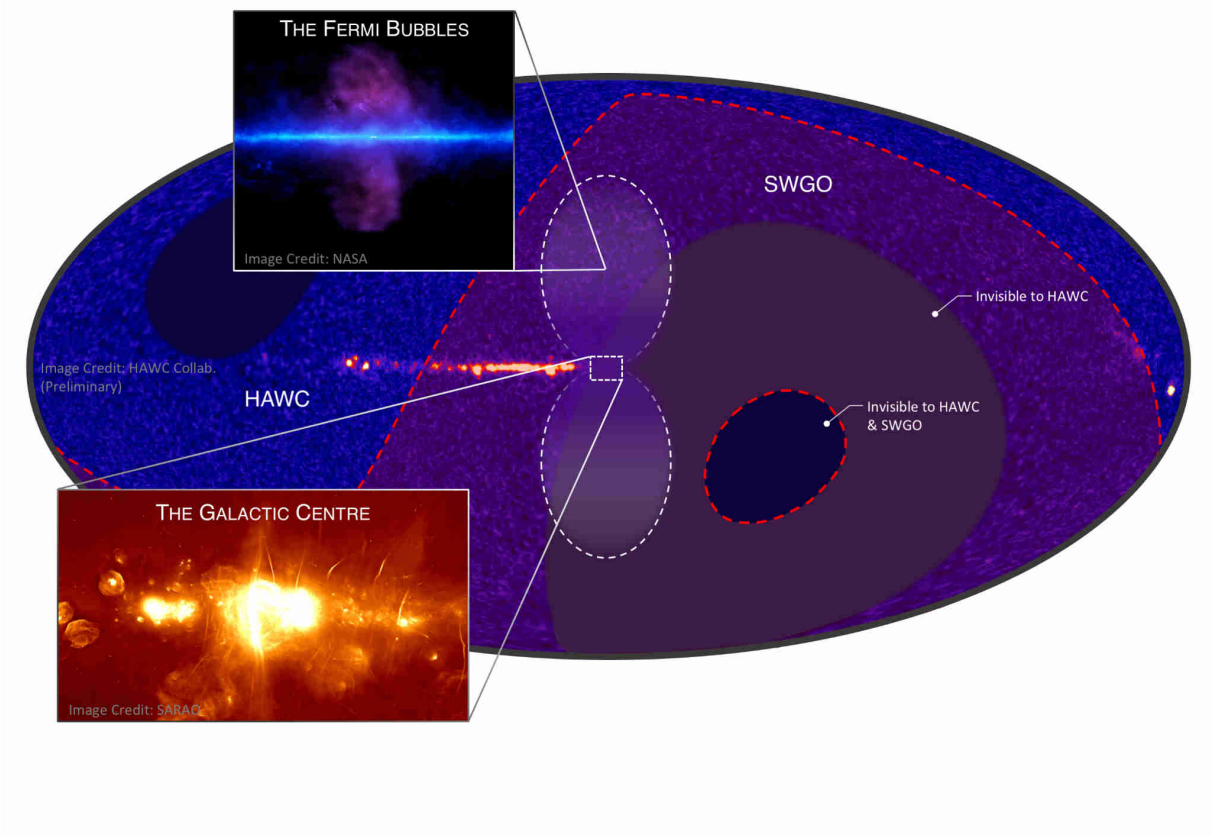

Figure 4: FoV of SWGO and HAWC.[26]

To fulfill these objectives, the observatory will be located in South America at a latitude of -30° to -10° and an altitude of 4.4 km or higher. The duty cycle shall be close to 100% and the field of view (FoV) shall be in the order of a steradian. The observatory will be composed by a high fill-factor core, with a larger area (and better sensitivity) with respect to HAWC, and a low sensitivity outer array, as shown in fig. 5.[26]

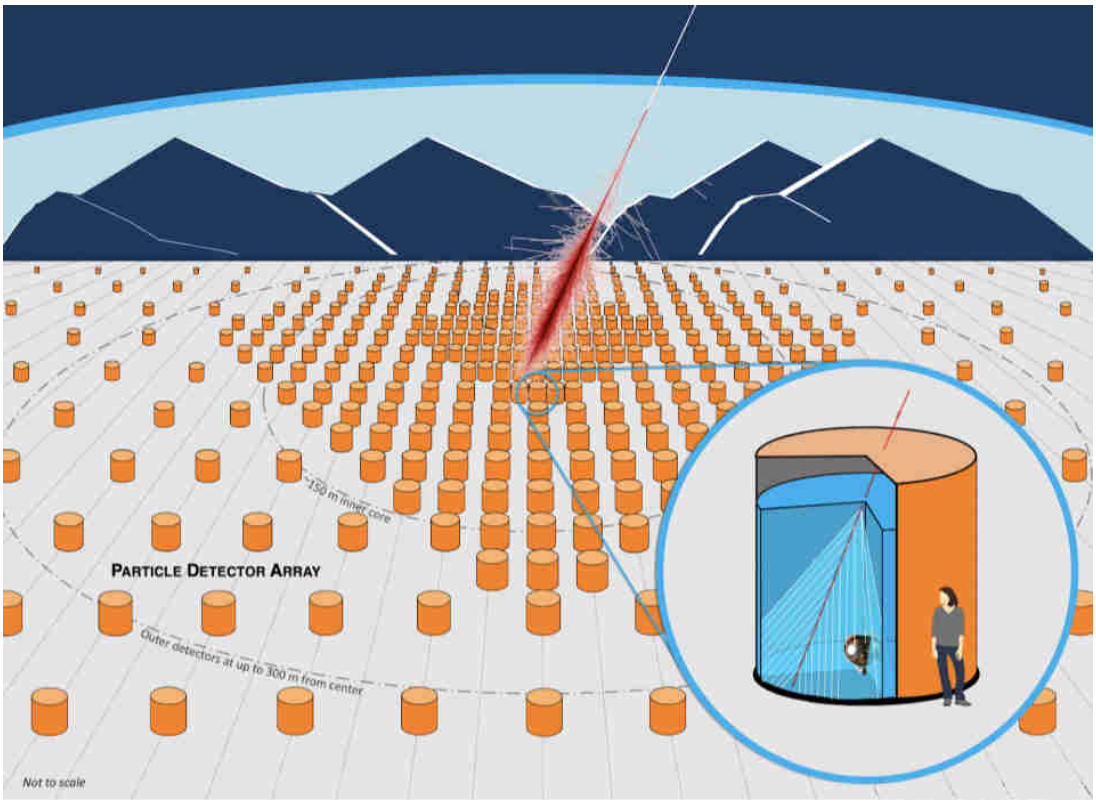

Figure 5: Qualitative representation of SWGO's layout.[26]

The detector will be based primarily on water Cherenkov units, for which design, three possible approaches will be evaluated (fig. 6):

- individual tanks (like HAWC)
- artificial ponds (like LHAASO's WCDA)
- in-lake deployment

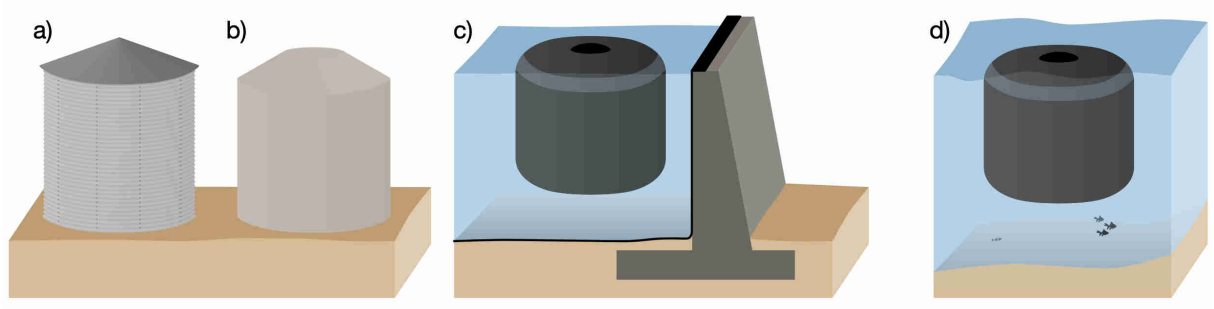

Figure 6: Detector concepts under study: cylindrical tanks constructed from (a) corrugated steel sheets or (b) roto-moulded HDPE; (c) open pond with floating bladder; (d) natural lake with floating bladder.[24]

0.3.1. The Cherenkov units

Cherenkov detectors are based, as the name says, on the Cherenkov effect: when a charged particle travels in a dielectric medium, its electric field causes the polarization of the atoms along the track (fig. 7). If the particle's speed is lower than the speed of light in that medium, the dipoles' arrangement is symmetric, resulting in a null dipole field, but if the speed of the particle is greater than the speed of light in the medium, the arrangement is asymmetric, so the dipole moment does not vanish and radiation is produced.[16, 27]

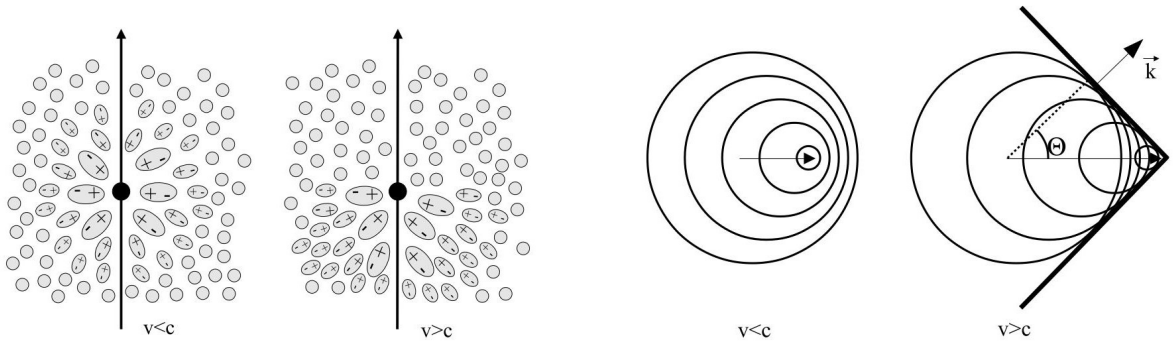

Figure 7: Left: polarization of the medium induced by the crossing of a relativistic particle. Right: Construction of Cherenkov wave-front.[30]

Detecting the radiation's photoelectrons (PE) allows, through their velocity and angle (see fig. 8), the assessment of the particle's characteristics.

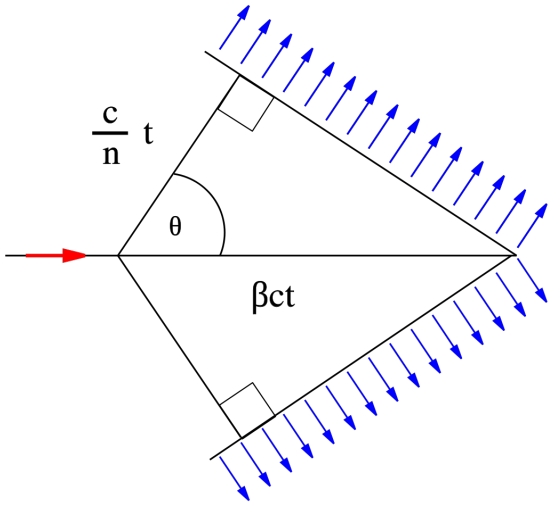

Figure 8: Scheme of the Cherenkov radiation's geometry. $c = 299792458 m/s$: speed of light in vacuum, n: refractive index of the medium, v_p: speed of the particle, t: time, Θ: emission angle, $\beta = v_p/c$ ratio between the speed of the particle and the speed of light.[48]

As mentioned in section 0.2 this technology is used in modern EAS detectors to provide an amplification effect and allow the PMTs to detect the particles which trajectory does not intersect them. Water is used as dielectric medium in these units: it is an excellent medium for converting the gamma rays into charged particles, that can be detected, and acts as a shield to electromagnetic particles, allowing the identification of muons in EAS of hadronic origin.[42]

There are several variables that have to be studied in the realization of this type of detector, such as the shape and dimensions of the tank, the type and position of the photosensors that will detect the Cherenkov light and the materials used. All these variables are being studied in order to design the Cherenkov units. For this purpose, both analytical and experimental means are being used by SWGO.

In this paper, the design and construction of a Cherenkov detector prototype for SWGO in Politecnico di Milano's labs will be discussed.

1 | The prototype tank project

As explained in section 0.3.1, there are many elements that have to be assessed in the design of the Cherenkov units. Many of them are being studied through simulation but, especially in the later design phases, some testing facilities will be required. The Italian SWGO partners (Politecnico di Milano, Università degli studi di Torino, Università degli studi di Padova, Università degli studi di Napoli and Istituto Nazionale di Fisica Nucleare (INFN)) have therefore decided to collaborate for the realization of one of such facilities at Politecnido di Milano (fig. 1.1).

(a) B6 building in Politecnico di Milano's Bovisa campus: site of the test installation and first candidate for the tank's location.

(b) The prototype tank inside B6 labs after test installation.

Figure 1.1: Initial site proposed for the prototype tank.

A variety of shapes are being considered for SWGO's Cherenkov units (circular base, hexagonal base, square base...)[11]; for this prototype, a cylindrical shape has been selected due to cost factors and also to minimize mechanical stress. The tank consists of a galvanized steel cylinder of 3.36 m diameter and 3.12 m height, to be covered internally with an AQUATEX® PVC cloth. This cover is removable, in order to allow the possibility of testing different materials on the inside of the tank. For example, reflective walls

allow a better detection capability, but they might extend the detection time due to the possible consecutive reflections of photons on the walls before they reach the PMTs. PVC cloth therefore gives a higher time resolution of the first photon but a lower detection efficiency.[11]

1.1. Project objectives

The main goal of of the prototype tank is being used as a testing facility for different configurations and different types of sensors.

The configuration planned to be used as reference is composed by:

- 1x 10" (253 mm) PMT situated in the center of the tank
- 4x 5" (128 mm) PMT equidistant from the center in square configuration

This is the first configuration to be tested in the tank. After that, testing different configurations will be possible, involving also experimental sensors.

In the universities of Padova and Napoli, alternative sensors' designs are being explored, such as wavelength shiftong materials applied to silicon photomultipliers (SiPM, Padova) and vacuum silicon photomultiplier tubes (Napoli).[32, 46] The prototype tank will serve as a testing facility for these designs.

The possibility of using external triggers to identify the entrance point of the particles in the tank, such as scintillators on the top, will also be studied.

The dimensions of the tank allow the division into two layers (fig. 1.2). The presence of the bottom layer is important for the identification of muons[1] and, even though at Milano's altitude muons will most likely be the only particles detected[22, 25, 38], performing some tests with a double layer configuration may produce useful results for the collaboration.

[1]Muons' measurements are important for the discrimination of the source of the shower (gamma-rays or hadronic cosmic rays). In hadronic showers, several percent of the particles reaching the ground are muons, which is not true in the case of gamma-rays.[1, 23] Heights from 0.5 m to 1 m of the lower layer are being studied for this purpose.[11] A schematic representation of muon detection in double layered tanks is showed in chapter 2, fig. 2.15.

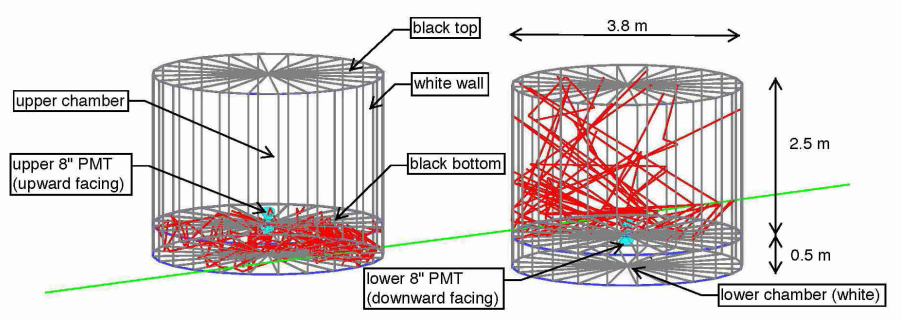

Figure 1.2: Cylindrical double layered WCD designs comprising an upper chamber ($\pi \times 1.91^2 \times 2.5\ m^3$) with white walls and black bases (top and bottom) and an entirely white lower chamber ($\pi \times 1.91^2 \times 0.5\ m^3$). The upper chamber comprises an 8" PMT facing upwards, and the lower chamber comprises an 8" PMT facing downwards. A Muon (green) passes through both units and produces photons (red).[29]

1.1.1. Project schedule

table 1.1 shows the schedule for the prototype tank, as it is at the time this report is being written; other points will be added as the project advances. Other sensors configurations and double-layer tests will be part of a later phase.

Prototype tank schedule

Schedule point	Period	Status
Order reference configuration PMT	Q4 - 2021	✓
Reference configuration PMT delivery	Q1 - 2022	✓
Tank installation	Q3 - 2022	in progress
Fill the tank with water	Q3 - 2022	to do
Start tests with the reference configuration	Q4 - 2022	to do
Start tests with novel sensors designs (Naples and Padova)	Q1 - 2023	to do

Table 1.1: The table shows the approximate schedule of the project; Q1, Q2, Q3, Q4 indicate the first, second, third and fourth quarter of the year.

The tank installation includes:

- tank construction (external metal cylinder + internal PVC cover)
- photomultiplier holder construction
- lifting system installation

1.2. Project requirements

1.2.1. The tank site

The original plan was to fill the tank with water up to 2.7 m for the tests and this would cause a pressure of 2.7 t/m^2 on the floor. These values could be increased in the case of double layer experiments. Such pressure would have to be supported by the installation site's floor for very long periods of time, so it was important to understand how much pressure could be exercised on the lab's pavement (B6 building lab: the first installation site considered) and how the detection capabilities of the Cherenkov unit could be affected by the water level. In addition to the pavement requirements, the installation site had to guarantee vertical space for both the tank and a lifting system for the detectors, as well as electric connections.

1.2.2. Water and materials

In order to guarantee the repeatably of measurements, purified water must be used in the tank. High water purity guarantees the lowest possible attenuation for UV Cherenkov light and, in addition to that, its properties can be well known and constant.[6] For this reason, purified water will be acquired and its purity shall not be compromised by any of the elements inserted in the tank. This posed a high constraint on the materials that could be used for the project. The PMTs, ordered from Hamamatsu, were of course already certified to be used in purified water, but a structure that would hold them in place had to be designed and built from scratch. Any part of the PMT holder structure and of the system that would place it in the water (and lift it up to change the test configuration) therefore had to be compatible with purified water. For the same reason, the tank had to be protected from the outside while not used, in order to minimize the amount of dirt entering the water.

A system to verify the water's purity should also be implemented and it could include periodic analysis of water samples.

1.2.3. The PMT holder

In order to fulfill the goals of the prototype tank described in section 1.1, it must be possible to test different types of sensors inside it, and to adjust the configuration following the tests' results, changing the sensors' position may be needed frequently. For this reason a structure (or multiple ones) was needed, capable of holding different sizes and shapes of

detectors in as many configurations as possible. Such structure had to be robust enough to handle the weight of the PMTs during tests and during placement. It should also possibly be economic and light-weighted in order to make the lifting easier. The need to change the PMT configurations implied that the design of both the holder and the lifting mechanism should be as simple as possible to interact with and that good placement precision should be achieved easily and in a short time.

2 | Study on particle detection as a function of the water level

Structural studies determined that the floor of Bovisa's B6 labs (chapter 1 fig. 1.1a, the first installation site considered) could handle safely a pressure of 2.0 t/m^2 for long periods of time, equivalent to a water level of 2.0 m, inferior to the originally planned 2.7 m (fig. 2.1). It was therefore of main importance to study the performance of the detector as a function of the water level. The objective of the study was to determine whether it was worth installing the tank in B6 labs with a lower water level with respect to the one originally considered (at least for single layer tests), or it would be preferable to find a different location. The results obtained could also be useful for the studies on tank geometries.

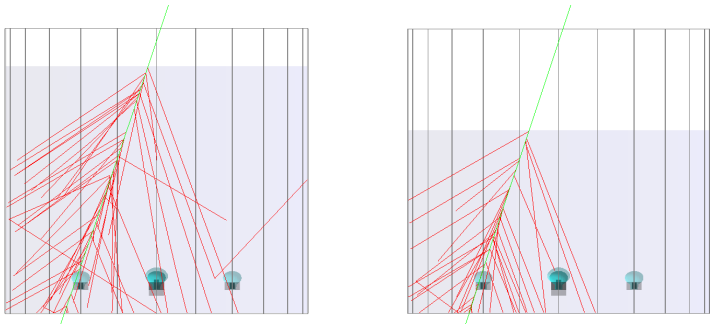

(a) Prototype tank with 2.7 m water level.

(b) Prototype tank with 2.0 m water level.

Figure 2.1: Visual output of the simulation of a muon (green) entering the tank and producing photons (red) in the two scenarios: original water level considered (a) and the reduced one (b).

2.1. Methods

As mentioned in section 1.1, at Milano's altitude, the only particles detected would most likely be muons. Accordingly with other simulation works on particle detection of the

SWGO collaboration, muons with 1 GeV and 10 GeV energies have been selected for the study[10, 11, 34]. 5 different water levels have been assessed for each energy: 1.65 m, 2.00 m, 2.35 m, 2.70 m and 3.05 m. Each water level and each energy required a separate simulation. The parameters analyzed as a function of the water level were[11]:

- detection efficiency
- number of photoelectrons detected
- standard deviation of the first photon time

The analysis and simulation framework of SWGO makes use of CORSIKA[21] and HAWCSim: the framework developed for HAWC, which uses Geant4[2] to simulate the particles' interaction with the tank itself and the water. The software simulates the Cherenkov photons' production caused by the particle's passage and their detection by the PMTs, collocated in the desired positions. Through this framework, a shower of different kinds of particles (e-, e+, μ-, μ+, γ, optical photons) and their interaction with the detector can be simulated.

A simulation has been performed for each energy value and water level of interest. The output of such simulation is a .root file, which can be analyzed in the root environment. For this procedure, a macro written in C++ and processed in the root environment has been used. The individual plots of each simulation's outputs have been produced too with the same method.

Finally, to put together the results of the various analyses done on the simulations with different levels of water and produce the final plots, libreoffice calc has been used. The outputs of this final procedure are the plots of the detection efficiency, number of PE detected and the standard deviation of the first photon time. (A more in-depth description of the simulation procedure and scripts in presented in appendix A.)

2.2. Setting the simulation

Firstly, the tank's geometry and materials have been set: a single layer cylindrical tank of 3.32 m diameter and 3.12 m height has been selected, with polypropilene as internal cover material. Secondly, the type and position of the PMTs had to be set. The 10" PMT was already implemented in HAWCSim, as well as an 8" PMT and a 3" PMT, but a 5" PMT was not available. To simulate the four 5" PMTs, 8" PMTs have been used, and then scaled to 5" during the analysis phase. The central 10" PMT has been assigned the ID number 1, and the four peripheral PMTs have been assigned the ID numbers 3, 5, 7,

9, as showed in fig. 2.2. The vertical position of the PMTs would depend on the holding system. An approximate height of 50 *cm* has been calculated for the head of the 10" PMT, which takes into account the detector's height and the cable's curvature. Hypothesizing that the holding system would hold the PMTs from their base, the 5" PMTs were placed such that their base's height coincided with the 10" base's height.

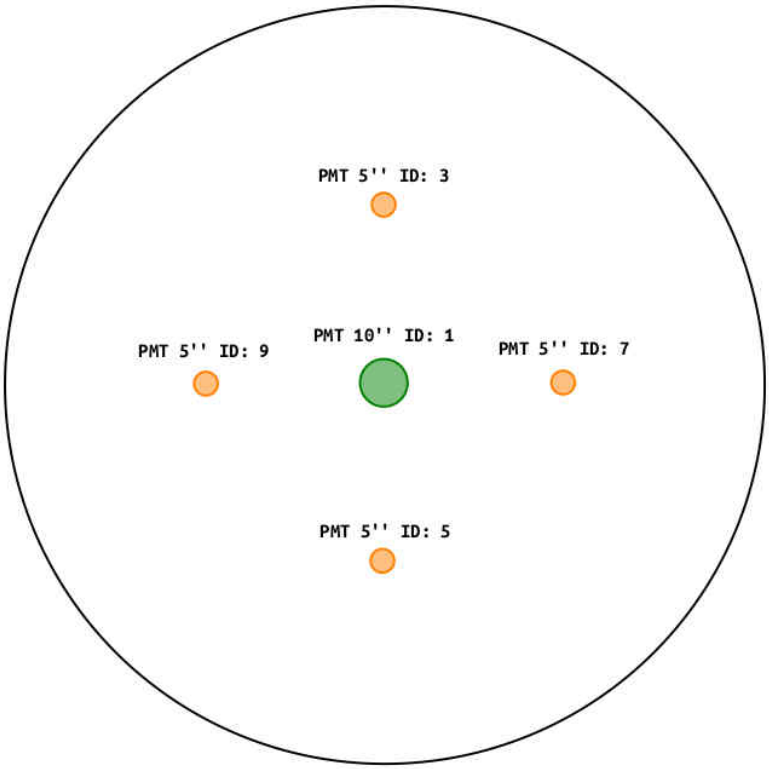

Figure 2.2: Scheme of the PMT disposition and ID.

2.2.1. Particle generation

In order to perform the simulation, it was necessary to generate the particles first. The muons have been generated with an azimuth angle ϕ in the range 0 - 360° and zenith angle θ extracted from the distribution $\cos^2\theta$[1].[11] 12000 particles have been generated in a disc of fixed radius ($r = 1.78m$, 10 *cm* larger than the tank's radius) and height ($h = 3.22m$, 10 *cm* larger than the tank's height) above the tank and, in the analysis phase, the first 10000 particles entering the tank have been considered. This was a necessary step in order to analyze 10000 particles for each energy and water level since not all the particles generated,

[1]It has been experimentally observed that the angular distribution of muons at sea level, for the energy range considered, can be approximately described as $\cos^2\theta$[14, 17, 19, 49]

having random movement direction, would enter the tank. The particle generation has been done using a macro created by Francesca Bisconti[10, 11], by giving it as inputs the data about the type of particles, their number and velocity, and the disc's radius and height. fig. 2.3 shows the generated particles' characteristics.

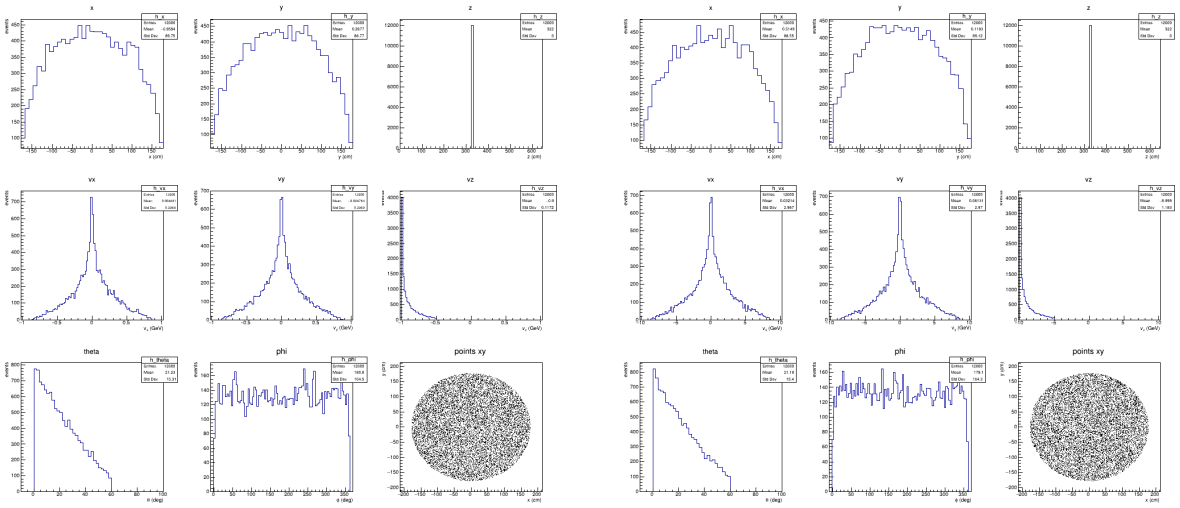

(a) 1 GeV muons generated.

(b) 10 GeV muons generated.

Figure 2.3: Plots of the generated particles characteristics: coordinates of the point where the particle is generated (x, y, z), components of the velocity (along x, y, z), zenith angle, azimuth angle and top view of the disc in which the particles are generated.

2.3. Analysis

The output of each simulation is a .xcd file, which can then be converted in .root. To extract the relevant data from the .root output files and analyze them, as previously done for particle generation, a C++ macro, run in the root environment, has been used. The script used is a modified version of Federico Montano's macro used for a similar simulation work.[34]

As explained in the previous section, in the analysis phase, 10000 particles have been considered among the ones entering the tank's water. Furthermore, among the PEs hitting PMTs 3, 5, 7 and 9, only the ones hitting the equivalent areas of the corresponding 5" PMTs have been analyzed. The analysis macro's outputs are some plots and a .csv file containing the quantities of interest for each simulation. Each time the analysis macro is run, it adds a line to the .csv file containing the selected parameters for each simulation. At the end of the process, this file contains all the data of interest of all the simulations performed.

2.3.1. Single simulations' results

At the end of the procedure just described, some plots are obtained for each simulation (one energy value and one water level). A rapid confrontation can be done between the plots of the same variable for the different water levels and a correlation can already be observed. In fig. 2.4 and fig. 2.5, for example, it can be seen that the number of PE detected is higher with a higher level of water.

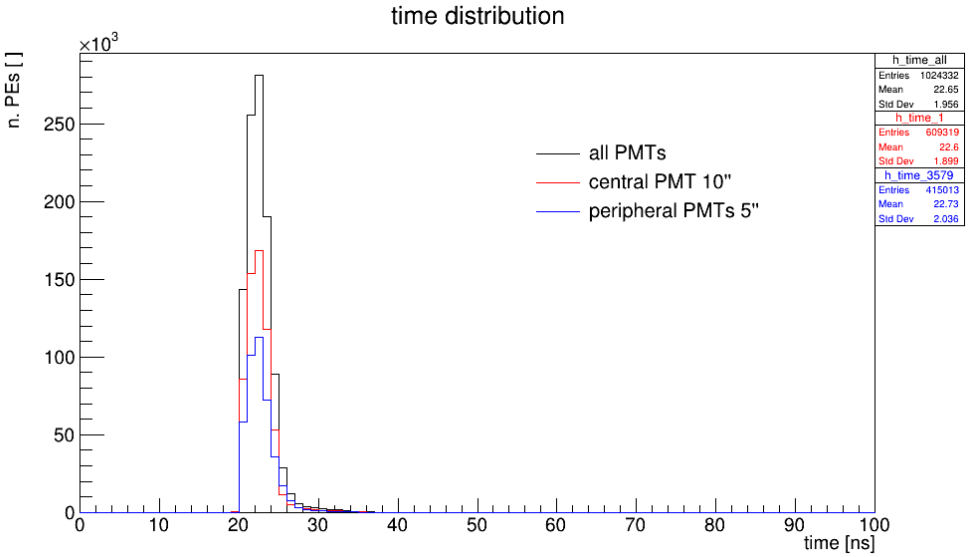

Figure 2.4: N. PE time distribution - Water level: 2.00 m. Total number of PE: 1024332.

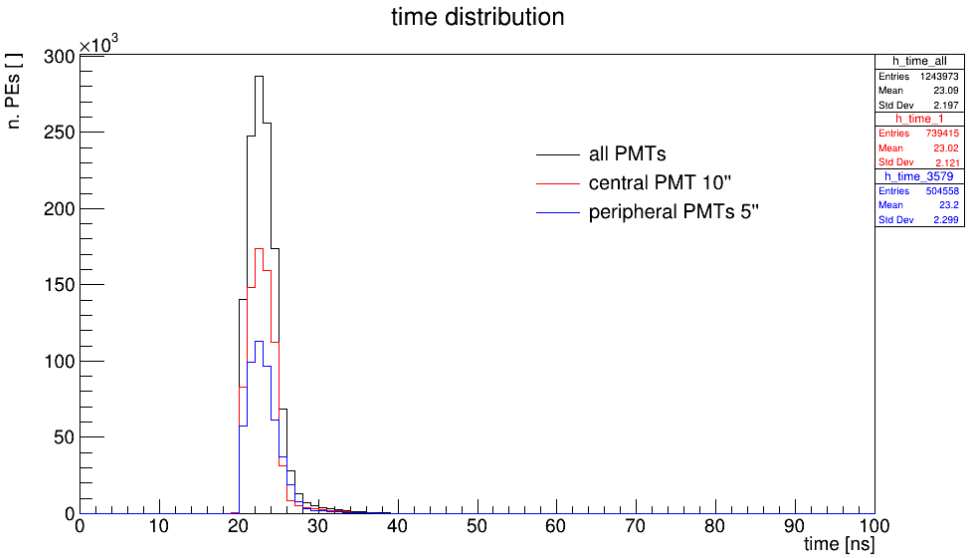

Figure 2.5: N. PE time distribution - Water level: 2.70 m. Total number of PE: 1243973.

In the following plots (fig. 2.6, fig. 2.7), most of the important analysis parameters can be observed, such as the number of particles analyzed, the number of particles reaching the water, the number of particles detected by the central and peripheral PMTs with and without coincidence. The coincidence is a parameter that can be used to verify the detection of a particle: a particle detection is considered valid only if at least two produced PE are detected by a PMT in an interval of 30 ns. It is a basic mechanism to ensure the reliability of a particle's detection.

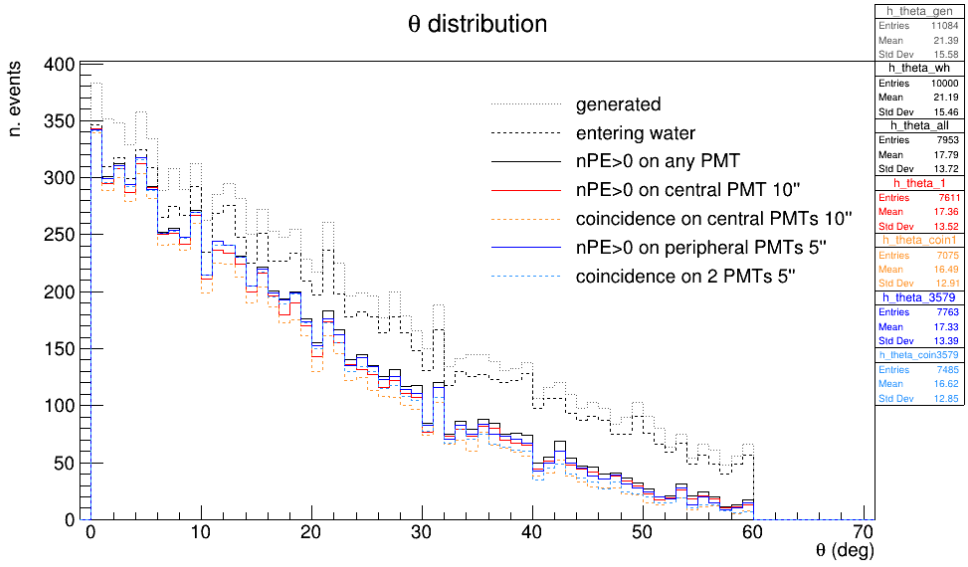

Figure 2.6: θ distribution of main quantities - Water level: 2.00 m.

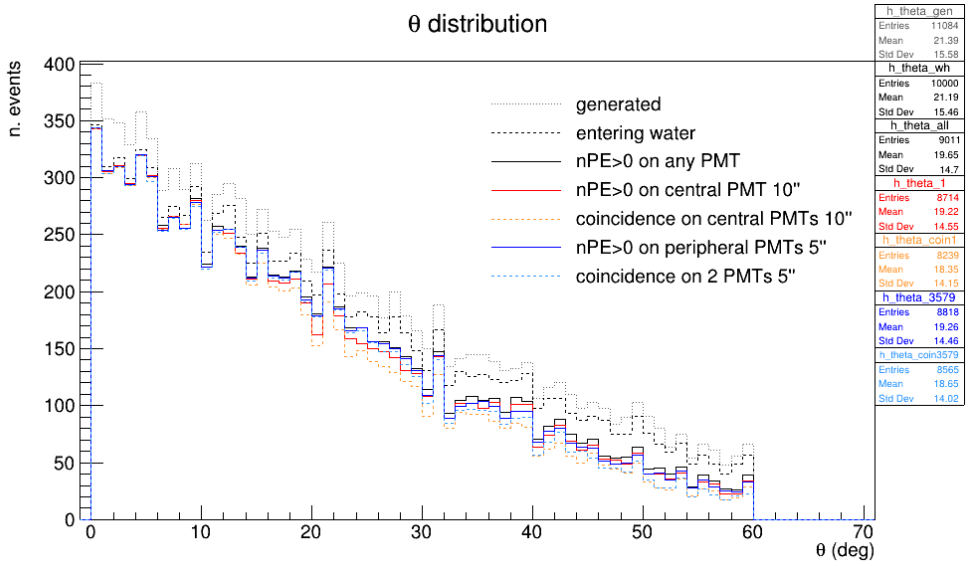

Figure 2.7: θ distribution of main quantities - Water level: 2.70 m.

2.3.2. Plots as a function of the water level

Even though the individual plots of each simulation were useful to have a first idea of how some parameters behave, the most important results for this study were obtained after an additional analysis step. In this phase, the results of all individual simulations have been analyzed together.

All the data had already been imported in the .csv file so it was sufficient to open it with libreoffice calc and elaborate the values to obtain the three parameters of interest for this analysis: detection efficiency, number of PE detected and standard deviation of the first photon time.[10]

Detection efficiency

Detection efficiency is the parameter that measures how many particles have been detected by a PMT configuration (n_{part}) with respect to the total number of particles entering the water (n_{tot}).

$$eff = \frac{n_{part}}{n_{tot}} \tag{2.1}$$

This parameter has been calculated in two cases: in the first one, n_{part} has been considered as the number of events that had produced at least 1 PE on the PMT configuration of interest (PMT 1 or PMT 3, 5, 7, 9 together), while in the second case, only events which had produced at least 2 PE within a 30 ns interval have been counted (coincidence). In both cases and for all energies and water levels, the number of particles entering the water was $n_{tot} = 10000$.

fig. 2.8 (no coincidence considered) and fig. 2.9 (coincidence considered) show the results comparing 1 GeV and 10 GeV muons. In both cases, detection efficiency increases linearly with the water level. Data for 2.00 m and 2.70 m in particular are confronted in table 2.1 and table 2.2.

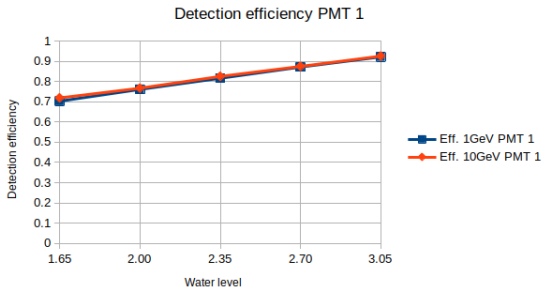

(a) Detection efficiency of the central PMT.

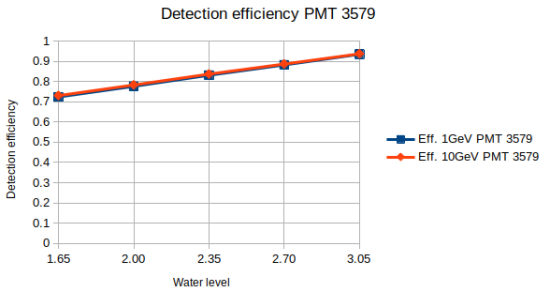

(b) Detection efficiency of the peripheral PMTs.

Figure 2.8: Detection efficiency shows a linear behaviour with the increase of the water level, no significant differences between 1 GeV and 10 GeV muons.

Summary table: detection efficiency

	PMT 1		PMT 3, 5, 7, 9	
	2.00 m	**2.70 m**	**2.00 m**	**2.70 m**
1 GeV	0.7611	0.8714	0.7763	0.8818
10 GeV	0.7670	0.8745	0.7829	0.8863

Table 2.1: Detection efficiency data for the two main water levels of interest.

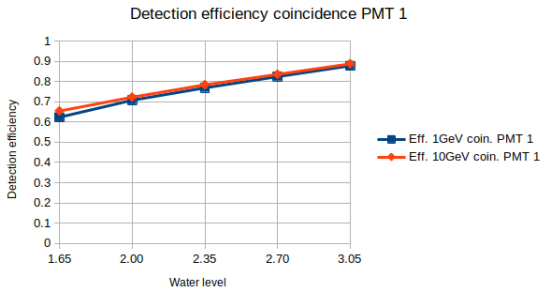

(a) Detection efficiency of the central PMT with coincidence.

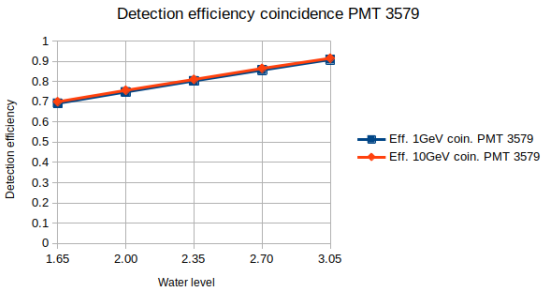

(b) Detection efficiency of the peripheral PMTs with coincidence.

Figure 2.9: Detection efficiency with coincidence shows a linear behaviour with the increase of the water level. No significant differences between 1 GeV and 10 GeV muons.

Summary table: detection efficiency with coincidence

	PMT 1		PMT 3, 5, 7, 9	
	2.00 m	**2.70 m**	**2.00 m**	**2.70 m**
1 GeV	0.7075	0.8239	0.7485	0.8565
10 GeV	0.7225	0.8352	0.7565	0.8645

Table 2.2: Detection efficiency with coincidence data for the two main water levels of interest.

Number of photo electrons

The second parameter analyzed has been the number of PE detected by each configuration (n_{PE}). The number has been scaled with respect to the number of particles entering the water ($n_{tot} = 10000$).

$$n_{PEscal} = \frac{n_{PE}}{n_{tot}} \tag{2.2}$$

This parameter measures the total number of PEs reaching each PMT configuration, regardless of which particles generated them, so coincidence is not considered. Also in this case, the values increase with the water level, as shown in fig. 2.10. Results for the two main water levels of interest are reported here too in table 2.3.

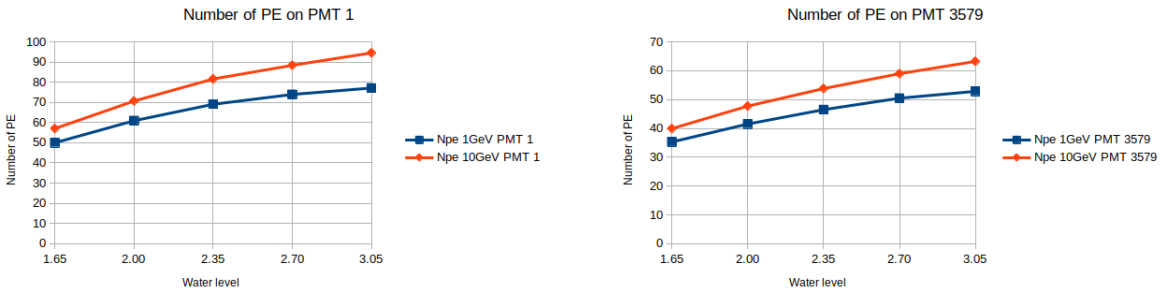

(a) Number of PE detected by the central PMT. (b) Number of PE detected by the lateral PMTs.

Figure 2.10: Number of PE detected, the behaviour is not linear anymore but still increasing with the water level. The number of PE detected is lower with 1 GeV muons with respect to 10 GeV.

Summary table: number of PE detected

	PMT 1		PMT 3, 5, 7, 9	
	2.00 m	**2.70 m**	**2.00 m**	**2.70 m**
1 GeV	60.9319	73.9415	41.5013	50.4558
10 GeV	70.6838	88.3816	47.7178	58.9565

Table 2.3: Number of PE detected data for the two main water levels of interest.

Standard deviation of the detection time of the first photon

The standard deviation (SD) of the detection time of the first photon, as its mean value, is a parameter which had already been calculated for each scenario during the individual analysis phase, as it can be seen in the legend side boxes of fig. 2.11.

The standard deviation measures how much the detection time values are close to their mean (dispersion), and it is an important parameter to observe since it gives an idea of how the detection precision varies with the water level.

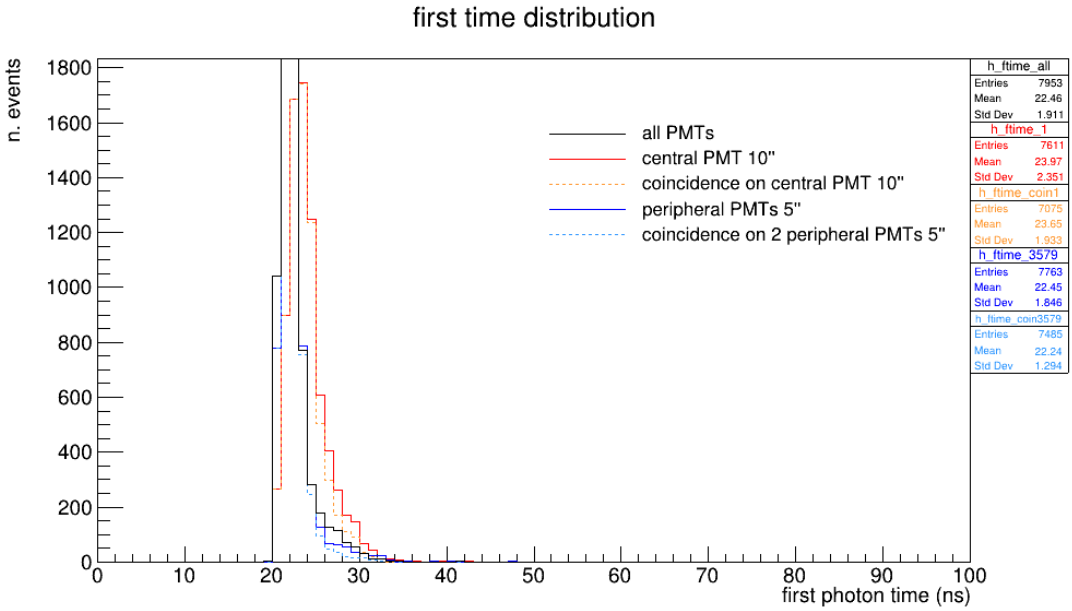

Figure 2.11: Detection time of the first photon for 1 GeV muons with 2.00 m of water.

The results show that the SD decreases with the water level (fig. 2.12, fig. 2.13), which means that the detector's precision gets better by increasing the water's height. table 2.4 and table 2.5 confront the values for 2.00 m and 2.70 m.

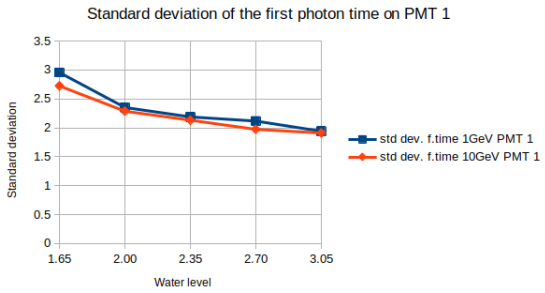

(a) SD of the first photon time for the central PMT.

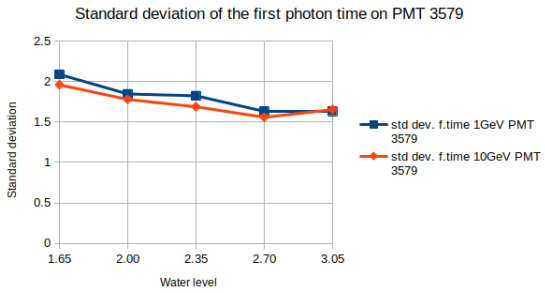

(b) SD of the first photon time for the peripheral PMTs.

Figure 2.12: SD of the first photon time, the quantity decreases with the water level. No significant differences between 1 GeV and 10 GeV.

SD of the first photon time

	PMT 1		PMT 3, 5, 7, 9	
	2.00 m	**2.70 m**	**2.00 m**	**2.70 m**
1 GeV	2.35132	2.11640	1.84644	1.63228
10 GeV	2.28702	1.97341	1.77844	1.55819

Table 2.4: SD of the first photon time data for the two main water levels of interest.

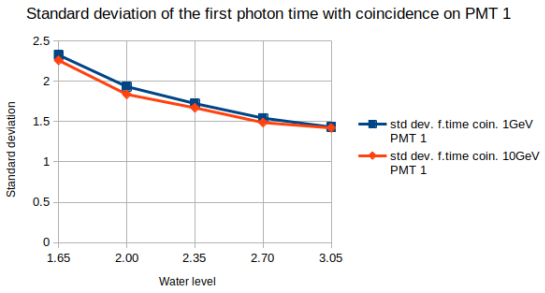

(a) SD of the first photon time for the central PMT with coincidence.

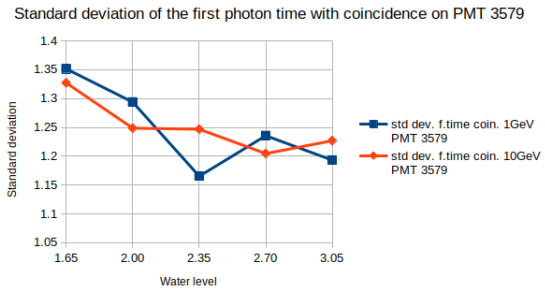

(b) SD of the first photon time for the peripheral PMTs with coincidence.

Figure 2.13: SD of the first photon time with coincidence, the quantity decreases with the water level. The behaviour for 1 GeV muons on the peripheral PMTs shows some irregularities.

SD of the first photon time with coincidence

	PMT 1		PMT 3, 5, 7, 9	
	2.00 m	**2.70 m**	**2.00 m**	**2.70 m**
1 GeV	1.93346	1.54286	1.29376	1.23555
10 GeV	1.83693	1.48762	1.24862	1.20444

Table 2.5: SD of the first photon time data for the two main water levels of interest.

Conclusions

It is clear from this analysis that the detection capabilities of the Cherenkov unit improve by increasing the water level. In particular, table 2.6 shows the percentage increase of detection efficiency between the 2.00 m reduced level scenario and the 2.70 m original scenario. The increase results to be of the ∼13-16%.

A more accurate study, for example considering more water levels, could be done to understand if the irregularities showed by SD (particularly for PMT 3579 with coincidence, fig. 2.13b) are just statistical fluctuations or if there are other factors that cause them.

Percentage increase of detection efficiency

	Muons 1 GeV	Muons 10 GeV
PMT 1	14.49%	14.02%
PMT 1 coin.	16.45%	15.60%
PMT 3579	13.59%	13.21%
PMT 3579 coin.	14.43%	14.28%

Table 2.6: Percentage increase in detection efficiency between 2.00 m and 2.70 m of water. The increase is slightly higher in the 1 GeV case.

All results have been submitted to some members of the SWGO collaboration and it has been decided to ask permission to install the tank outside the lab in order to maximize the detector's performances and allow eventual future tests with double layer configurations (fig. 2.14).

(a) Final site for the prototype tank: from afar. (b) Final site for the prototype tank: detail.

Figure 2.14: Final site for the prototype tank: close to B14 labs, where the PMTs signals will be received.

2.4. Electrons simulations

In order to verify the model, it has been decided to perform a series of simulations with electrons too. Muons are more penetrating particles with respect to electrons: the latter lose energy faster, thus producing Cherenkov light only during a brief segment in the upper part of the detector; muons on the other hand usually cross the whole tank.

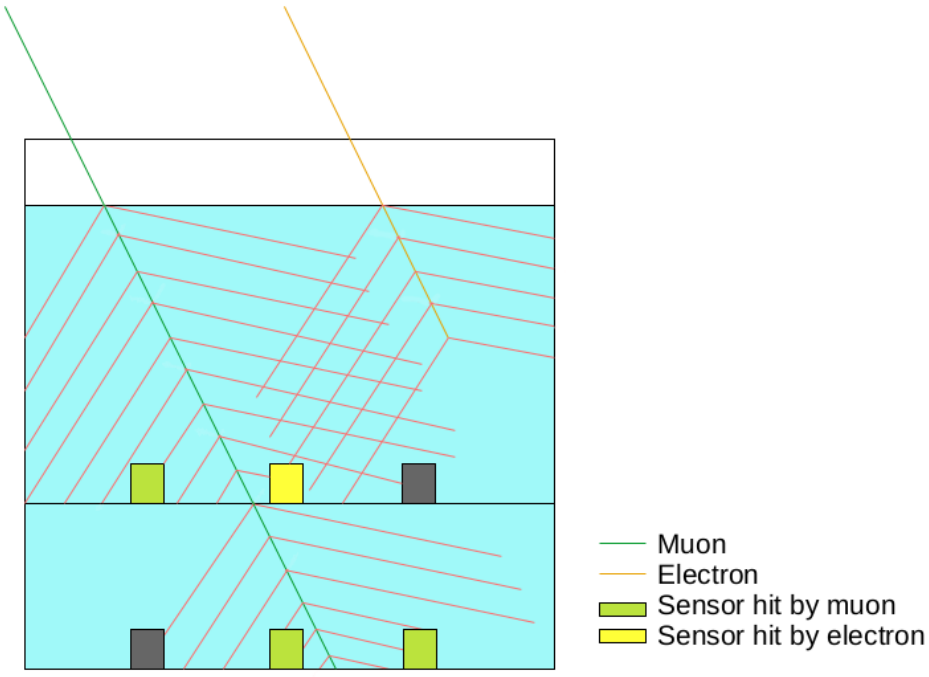

Figure 2.15: Scheme of muon identification with double layer tank.

This characteristic is in fact exploited in double layer tanks to identify muons: they are the only particles able to reach the lower layer (fig. 2.15). Simulating electrons' showers in a single layer tank, a lower number of PE detected by the PMTs can be expected with a higher water level since they are produced only in the upper part of the tank and many of them would therefore be absorbed by the water before reaching the photosensors. If the model is correct, this should be seen in the number of PE detected and in the efficiency values.

Electrons with an energy of 1 GeV have been selected for this study, in order to confront the results with the ones obtained with 1 GeV muons.

The procedure has been the same one used for the muons: the shower has been generated in a disk over the tank and then a simulation has been carryed out for each water level.

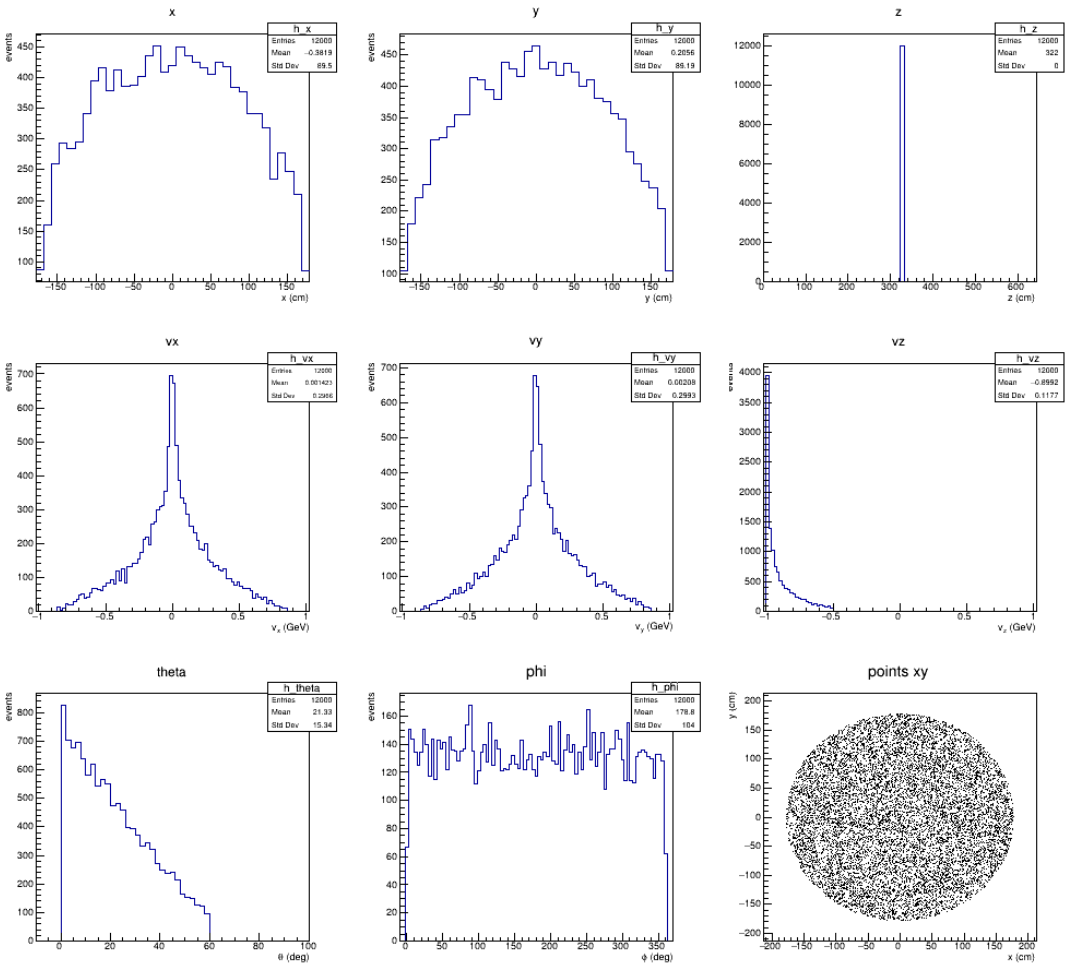

Figure 2.16: Plots of the generated e- characteristics: coordinates of the point where the particle is generated (x, y, z), components of the velocity (along x, y, z), zenith angle, azimuth angle and top view of the disc in which the particles are generated.

2.4.1. Plots as a function of the water level

As for the muons, at the end of the analysis phase, all data from the 5 water levels' simulations were available in a .csv file, so they have been elaborated in Libreoffice calc to obtain the plots of detection efficiency, number of PE detected and SD of the first photon time.

Detection efficiency

Efficiency's behaviour for 1 GeV electrons looked very similar to the one for muons (fig. 2.17, fig. 2.18). To better compare the results, the angular coefficients of the lines resulting from the plots have been computed. For this calculation, the line passing through the first and last points (1.65 m and 3.05 m) of each plot has been considered (table 2.7).

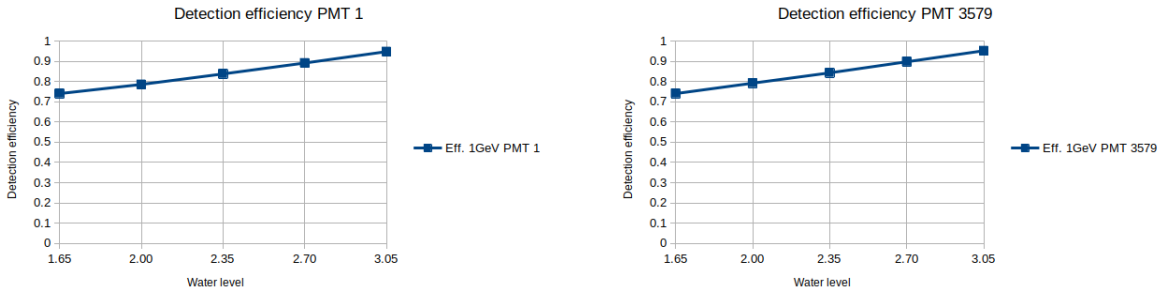

(a) Detection efficiency of the central PMT.

(b) Detection efficiency of the peripheral PMTs.

Figure 2.17: Detection efficiency shows a linear behaviour with the increase of the water level, as in the muons case.

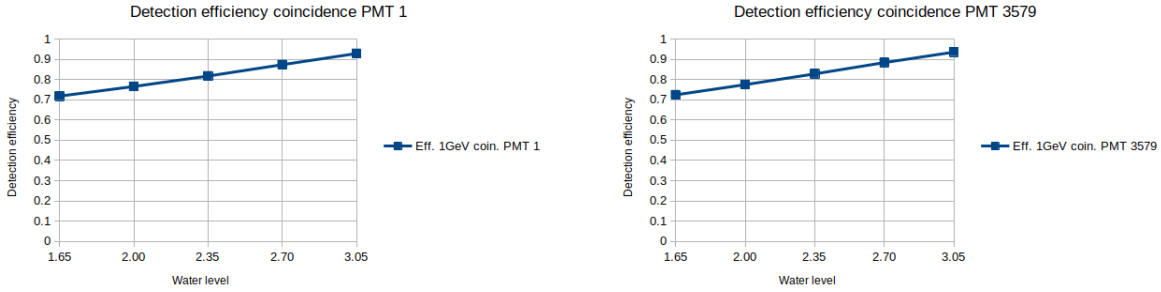

(a) Detection efficiency of the central PMT with coincidence.

(b) Detection efficiency of the peripheral PMTs with coincidence.

Figure 2.18: Detection efficiency with coincidence shows a linear behaviour with the increase of the water level, as in the muons case.

Angular coefficients comparison: detection efficiency

	Muons 1GeV	Electrons 1GeV
PMT 1	0.1564	0.1479
PMT 3579	0.1506	0.1511
PMT 1 coin.	0.1815	0.1503
PMT 3579 coin.	0.1544	0.1509

Table 2.7: Comparison between the angular coefficients of the plot lines of detection effciency for the muons and electrons case: they result to be lower for electrons except for the peripheral PMTs in the case without coincidence.

As it can be noted in the table, the angular coefficient results to be lower in the electrons case except for the peripheral PMTs when coincidence is not considered.

Number of photo electrons

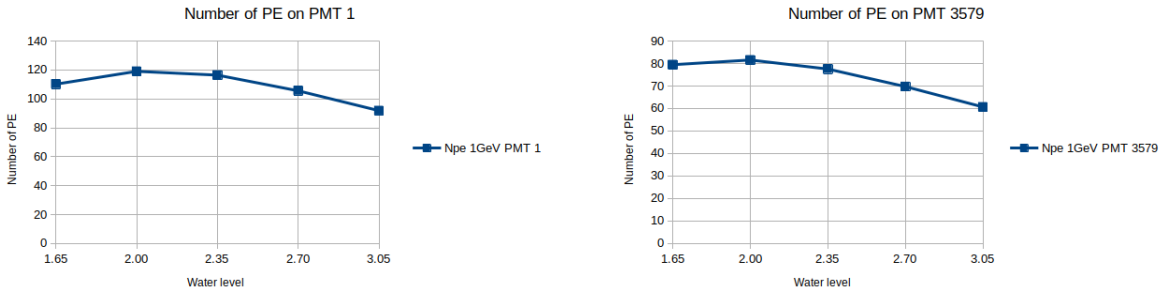

(a) Number of PE detected by the central PMT. (b) Number of PE detected by the lateral PMTs.

Figure 2.19: Number of PE detected: the values initially increase with the water level and decrease after 2.00 m.

For both the central and the peripheral PMTs, the number of PE detected increases with the water level up to 2.00 m and then decreases, as shown in fig. 2.19. This is compatible with the energy loss of electrons travelling through water.

Standard deviation of the detection time of the first photon

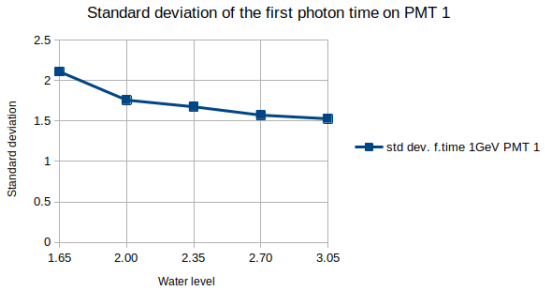

(a) SD of the first photon time for the central PMT.

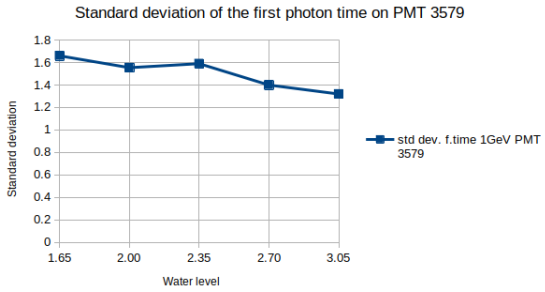

(b) SD of the first photon time for the lateral PMTs.

Figure 2.20: SD of the first photon time: the quantity decreases with the water level.

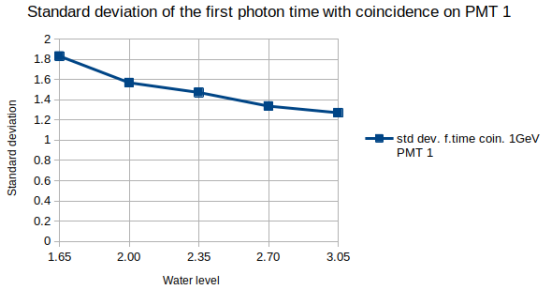

(a) SD of the first photon time for the central PMT with coincidence.

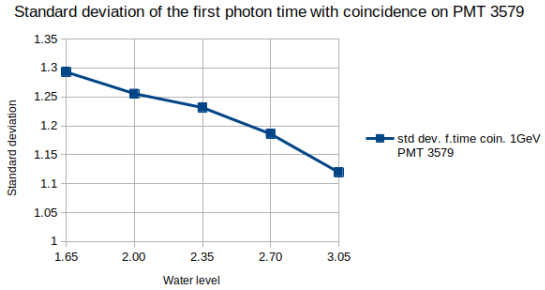

(b) SD of the first photon time for the lateral PMTs with coincidence.

Figure 2.21: SD of the first photon time with coincidence: the quantity decreases with the water level.

The behavior showed in fig. 2.20 and fig. 2.21 is similar to the one showed by muons. As for the case of detection efficiency, calculating the angular coefficients can be useful to better assess the differences between the muons' and the electrons' results. The SD's behaviour is not linear, but the line passing through the first and last point can be considered as a rough approximation. table 2.8 shows that the SD of the first photon's time decreases faster for muons except in one case.

Angular coefficients comparison:

	Muons 1GeV	Electrons 1GeV
PMT 1	-0.7244	-0.4154
PMT 3579	-0.6376	-0.3996
PMT 1 coin.	-0.3241	-0.2427
PMT 3579 coin.	-0.1132	-0.1239

Table 2.8: Comparison between the approximate angular coefficients of SD's plots for muons and electrons: their absolute value results to be lower for electrons except for the peripheral PMTs in the coincidence case.

Conclusions

The results seem to be coherent with theoretical expectations, so the model can be considered to be good. It is possible that, in a bigger tank, for higher water levels, the detection efficiency could decrease and, in general, the observed effects could be more evident. If the detector will have to be used for a variety of particles (not just muons), a compromise will have to be found for the water level in order to optimize the performances for all particles.

3 | Design of the PMT holder

In addition to the reference configuration (1x 10" PMT + 4x 5" PMT), some other possible testing configurations had been hypothesized (fig. 3.1). Designing single structures to hold and place separately each PMT was an option, but position precision would be difficult to achieve: it would require a lifting system able to move horizontally (and not just vertically) with high accuracy. Furthermore, a system to attach and remove the chains or ropes used for lifting (once placed the PMT underwater) could be needed to reduce the quantity of objects in the water over the sensors, which may interfere with photon detection. Using a single big structure instead would allow a simpler lifting system: the accuracy of the relative distances between the detectors would be assured by precise placing out of the water and the centering with respect to the tank would be guaranteed during the installation phase of the lifting system itself. In addition to that, the number of chains/ropes used would be way lower and it would be sufficient to rest them on the tank's walls after the structure's placement, without any need for detachment mechanisms.

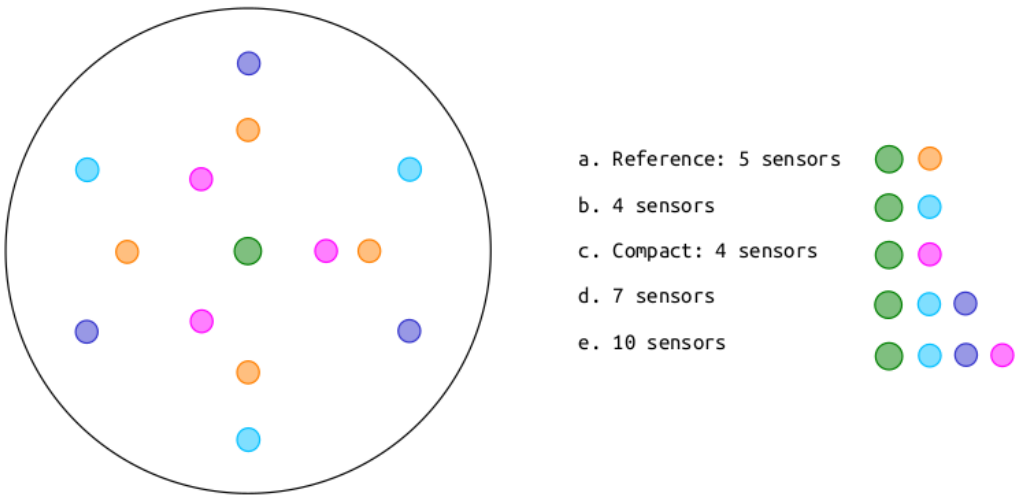

Figure 3.1: Scheme of the example potential configurations that could be tested in the prototype tank.

3.1. Methods

The design started from the materials' requirements: the material's properties would influence the shapes and thicknesses allowed for the structure. After making a list of candidate materials (see appendix B), the concept design phase started, where possible shapes for the structure and lifting systems have been considered until an optimal solution has been found.

A 3D model has been realized in SolidWorks in order to perform a loading simulation on the structure and choose the adequate thickness for the parts.

After approving the design, the structure has been manufactured in Politecnico's workshop (Bovisa campus, fig. 3.2).

(a) Politecnico's workshop (metallurgy section). (b) Cutting (right) and bending (left) machines.

Figure 3.2: Politecnico's Bovisa campus workshop: general view and machines used.

3.2. Materials

In order to keep precise fixed distances between the PMTs, the holder structure had to be made of a stiff material. Some flexibility could also be useful to accommodate different sizes of detectors. For these reasons, metals were the best candidates. Aluminum and stainless steel were considered as main alternatives since they are easily available on the market. Aluminum however can show corrosion after long periods of time, especially if not pure and if cracks form,[39, 45] so stainless steel was chosen.

A gasket would be needed around the PMTs for better holding and in order not to press the metal directly on them. The idea was to use a rubber material (such as, that could

also be applied under the structure to avoid direct contact between the metal and the PVC cloth, which could be ruined by it.

Since it may be needed to change the sensors' configuration frequently, a simple lifting system had to be designed, and the chains or ropes used to hold the structure would need to be compatible with the water. The low estimated weight of the structure allowed the choice of polypropylene ropes, which are cheaper with respect to steel chains, lighter and are of course compatible with purified water.

3.3. The hexagonal holder

The second design step was finding a shape for the structure that could allow the highest variety of PMTs configurations in order to be used for all the experiments contemplated for the tank. This meant that the structure had to be able to hold in place PMTs of different dimensions in as many different positions as possible but still have a limited weight to make it easy to lift it up and down. The structure had to be simple too and made with a low variety of pieces in order to make it easier to find them on the market or to produce them.

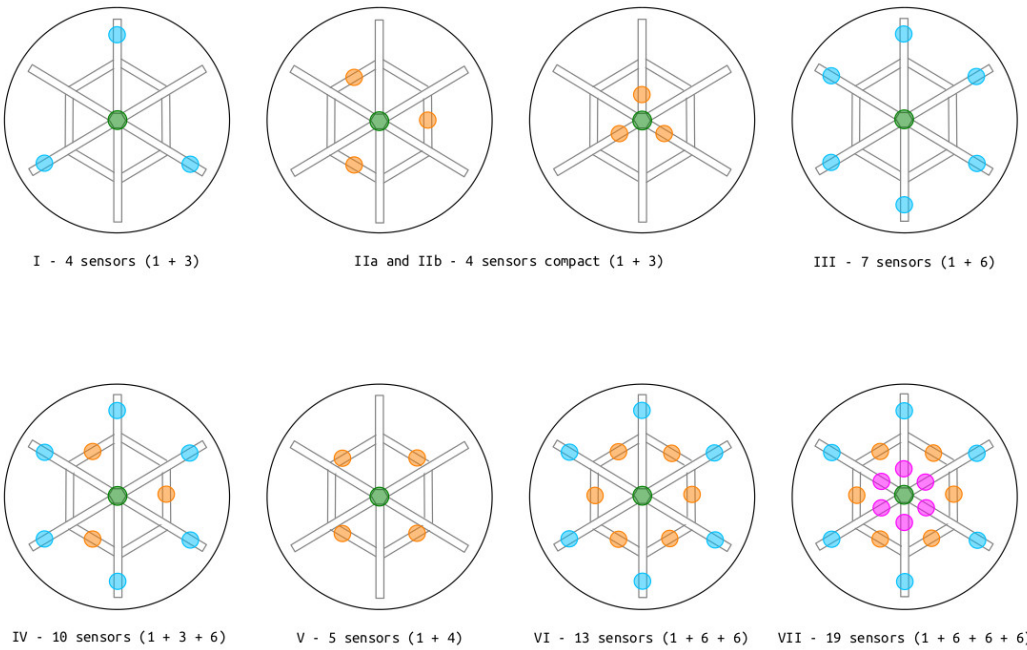

Figure 3.3: Possible PMT configurations assessed for the hexagonal holder.

After a few drafts, an hexagon-like structure has been selected since it was able to provide configurations with three PMTs on the same radius, four PMTs on the same radius and six PMTs on the same radius, all keeping one central larger PMT (fig. 3.3). The six long radii allow flexibility in the distances for the three and six PMTs configurations. The hexagon has been designed to hold the four PMTs configuration such that they are placed at half the tank radius, which is the configuration that has been planned to be the reference for this prototype (fig. 3.4).

In order to have maximum flexibility and simplicity for the positioning of the PMTs, perforated flat bars have been used in the design; this also contributes to making the structure more light-weighted. The holes allow the insertion of long screws to be used for holding the PMT.

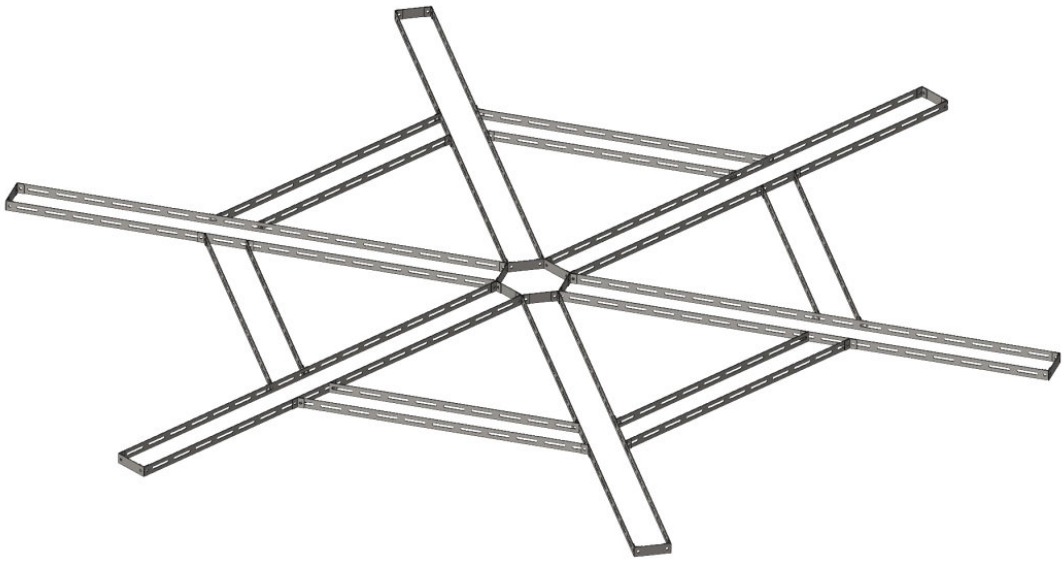

Figure 3.4: 3D model of the hexagonal holder created in SolidWorks.

An important constraint was the structure's distance from the bottom of the tank. The PMTs' cables have in fact a minimum curvature angle that has to be respected for their correct functioning and preservation (see fig. 3.5, full-scale images can be found in appendix C). For this reason, some sustains were necessary since keeping the structure suspended with ropes was not optimal for the aforementioned field of view related reasons. The minimum height of the structure from the bottom has been set to 15 cm to allow the correct curvature of the cables and some margin.

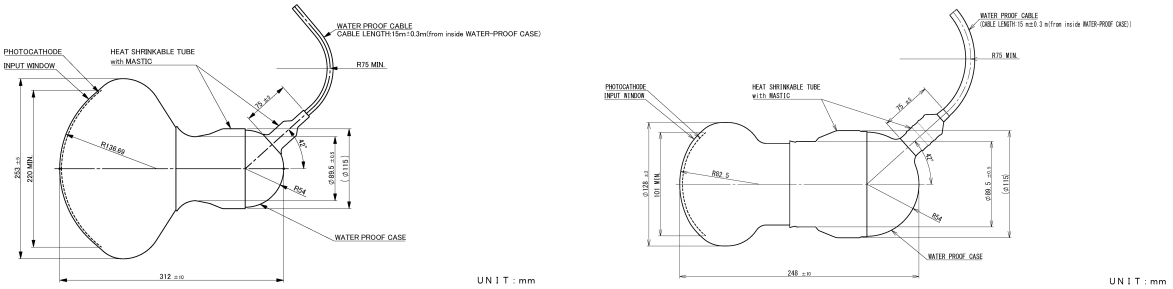

(a) R701-Y006 (10” PMT) (b) R6594-Y004 (5” PMT)

Figure 3.5: Schematics of the Hamamatsu PMTs of the reference configuration.

In order to protect the tank’s PVC cover (or other eventual liners used in further tests), a metal piece in contact with it had to be avoided, so the first idea had been to use a plastic material for the supports. In later design steps however, the supports have been converted to stainless steel, since they would be simpler to produce, with a rubber layer on the bottom to avoid contact with the cover.

It was necessary to guarantee the capability of the structure of holding the PMts without relevant deformation, so some simulations have been carried out in SolidWorks. The weight of the PMTs has been introduced by placing some glass discs in the positions planned for the detectors, which have been virtually loaded with the sensors’ mass. The simulations showed that the hexagonal holder could handle the weight of configuration VII (corresponding to full load: fig. 3.3) with negligible resulting displacement (fig. 3.6b) and a large margin on the yield stress (fig. 3.6a). The maximum values reached are reported in table 3.1, together with the PMTs’ masses and the material’s yield stress.

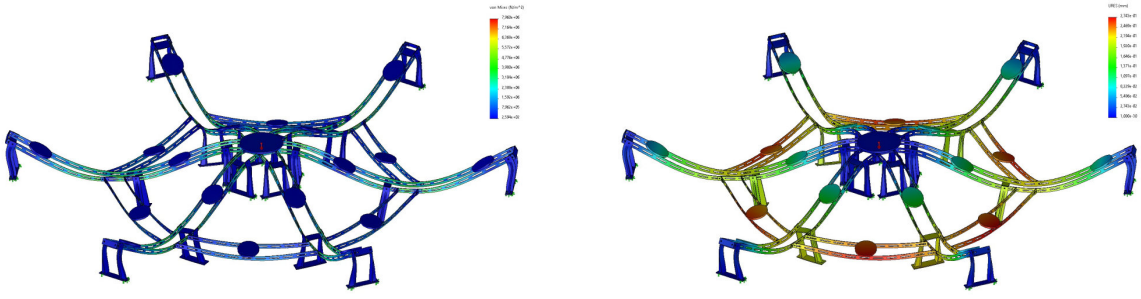

(a) Von Mises stress with static maximum load. (b) Displacement with static maximum load.

Figure 3.6: Hexagonal holder: results of the solidworks static analysis.

Static analysis parameters

Parameter	Real value	Margin
R701 mass	2.90 kg	+15%
R6594 mass	2.07 kg	+15%
AISI 304 yield stress	8,07×10^{8} N/m^2	-
Maximum stress reached	7.96×10^{6} N/m^2	-
Maximum displacement reached	2.743×10^{-1} mm	-

Table 3.1: Hexagonal holder: static analysis data. A 15% margin has been considered on the PMTs mass to account for the mass of the cable.

3.4. The cross holder

The hexagonal holder design represented the best compromise found between weight, robustness and number of configurations that could be handled. The steel bars needed for it however were not available on the market as they had been designed (dimensions, materials, type of holes...) and so two options were available: ordering custom parts, which would take a higher time and price, but would allow to produce exactly the designed structure; or adapting the design to the parts available on the market, which was quicker and more economic but would require some compromises. The second option was chosen and, since at the time (March 2022) the 5 reference configuration PMTs were nearly ready to be tested while the other designs were still in development, it has been decided to produce a smaller temporary structure to test the 10" and four 5" PMTs, with the idea of disassembling it later and use the pieces for the original larger one. This smaller structure would be able to hold the reference configuration PMTs with more flexibility on the 5" distance from the tank's center and it would be easy to assemble and disassemble. A cross-like structure has been designed (fig. 3.7), using 1 m long perforated flat bars already available on the market and two other types of pieces obtainable from the same bars by cutting and folding them (fig. 3.8, technical drawings and measures of the parts in appendix D).

Also in this case, a loading simulation has been carried out in SolidWorks, this time just with the 5 reference PMTs (fig. 3.9). The results confirmed that the structure was able to hold the PMts in place with nearly null deformation and large margin on the yield stress, so the design has been approved (table 3.2).

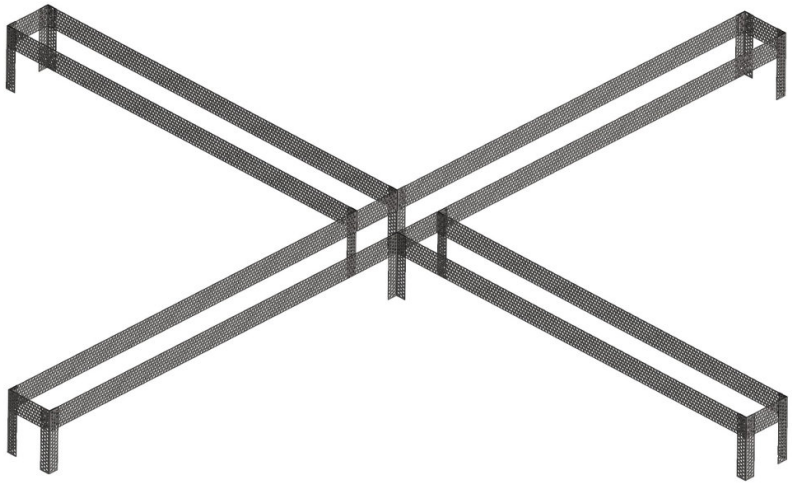

Figure 3.7: 3D model of the cross holder.

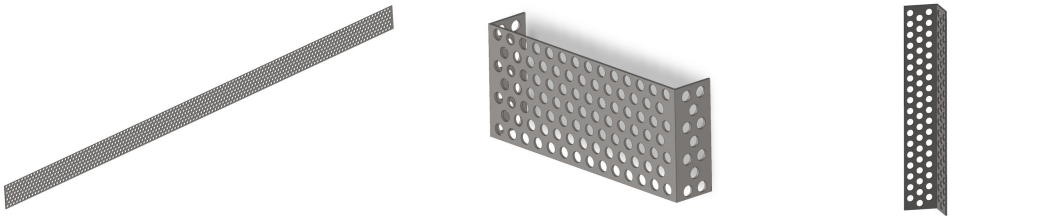

(a) Part a: flat bar. (b) Part b: C-profile. (c) Part c: L-profile.

Figure 3.8: Parts composing the cross holder: part a is the base piece bought from the supplier (1000 mm x 50 mm x 1 mm perforated flat bar) from which part b and part c can be obtained.

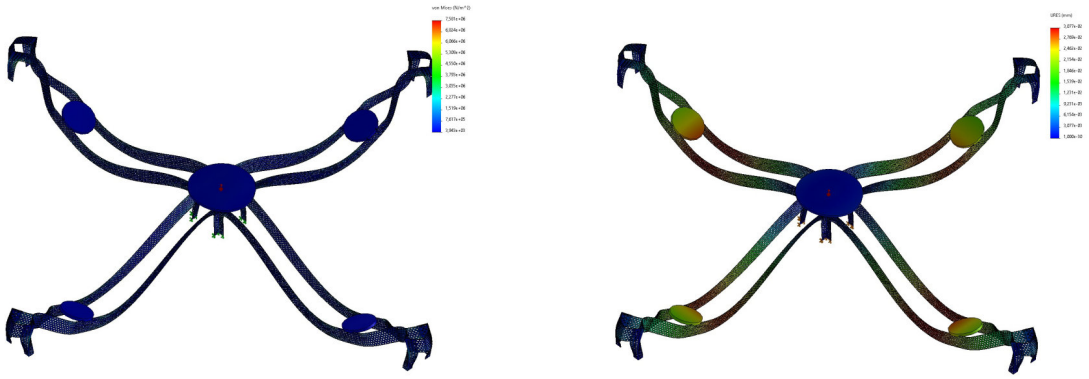

(a) Von Mises stress with static maximum load. (b) Displacement with static maximum load.

Figure 3.9: Cross holder: results of the solidworks static analysis.

Static analysis parameters

Parameter	Real value	Margin
R701 mass	2.90 kg	15%
R6594 mass	2.07 kg	15%
AISI 304 Yield stress	8,07×10^8 N/m^2	-
Maximum stress reached	7.581×10^6 N/m^2	-
Maximum displacement reached	3.077×10^{-2} mm	-

Table 3.2: Cross holder: static analysis data.

As for the hexagonal holder, the original plan was to use long screws that applied pressure on a gasket around the PMTs to hold them in position (fig. 3.10a). Considering the availability of the materials however, it has been decided to use 2 C-profiles (fig. 3.8b) for each PMT to guarantee higher stability (fig. 3.10b).

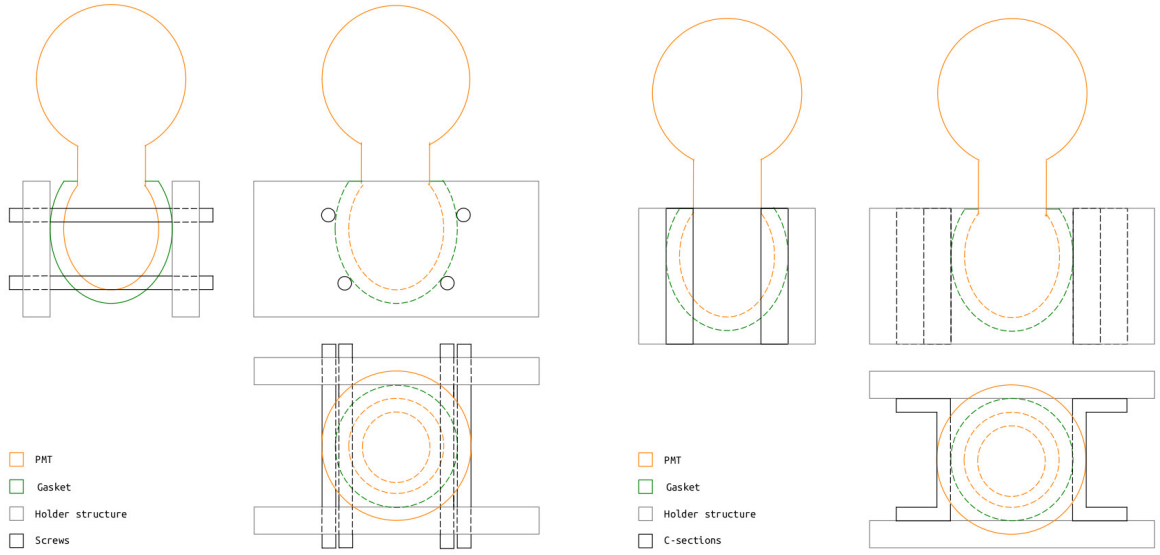

(a) PMT holding method with screws.

(b) PMT holding method with C-profiles.

Figure 3.10: Schematic drawings of the two methods for holding the PMTs (not in scale).

3.4.1. Structure manufacturing

Some perforated flat bars in stainless steel AISI 304 (corresponding to part a, fig. 3.8a) have been acquired to create the parts required for the structure. The pieces needed for the realization of the cross holder were:

- 8 flat bars (fig. 3.8a)
- 16 C-profiles (fig. 3.8b)
- 12 L-profiles (fig. 3.8c)

The C-profiles and the L-profiles could be obtained by cutting and folding the original perforated flat bars. The work has been done in Politecnico's workshop (fig. 3.11).

(a) Steel short bar in the bender.

(b) L-profile after bending.

Figure 3.11: Bending of the L-profiles for the PMT holder in Politecnico's workshop.

After manufacturing the parts, a single arm of the cross holder has been built in order to test its robustness and stability when loaded (fig. 3.12). The parts were held together with stainless steel bolts.

(a) Single arm of the cross holder

(b) Position of the 5" PMT

Figure 3.12: First test building of a single arm of the cross holder.

The test building was successful, so it has been decided to proceed with the whole structure. The holes have been enlarged where needed to obtain a more precise assembly. Then the parts have been carefully cleaned with acetone in order not to leave manufacturing residues on them (this procedure will be repeated before immersing the structure in purified water).

3.4.2. PMT placement

When the structure was complete, a placement test with the five reference configuration PMTs has been done. The appropriate rubber for the gaskets, compatible with purified water, had not been ordered yet, so foam rubber has been used (fig. 3.13). The structure was not deformed by the PMTs' weight and the sensors were held stably.

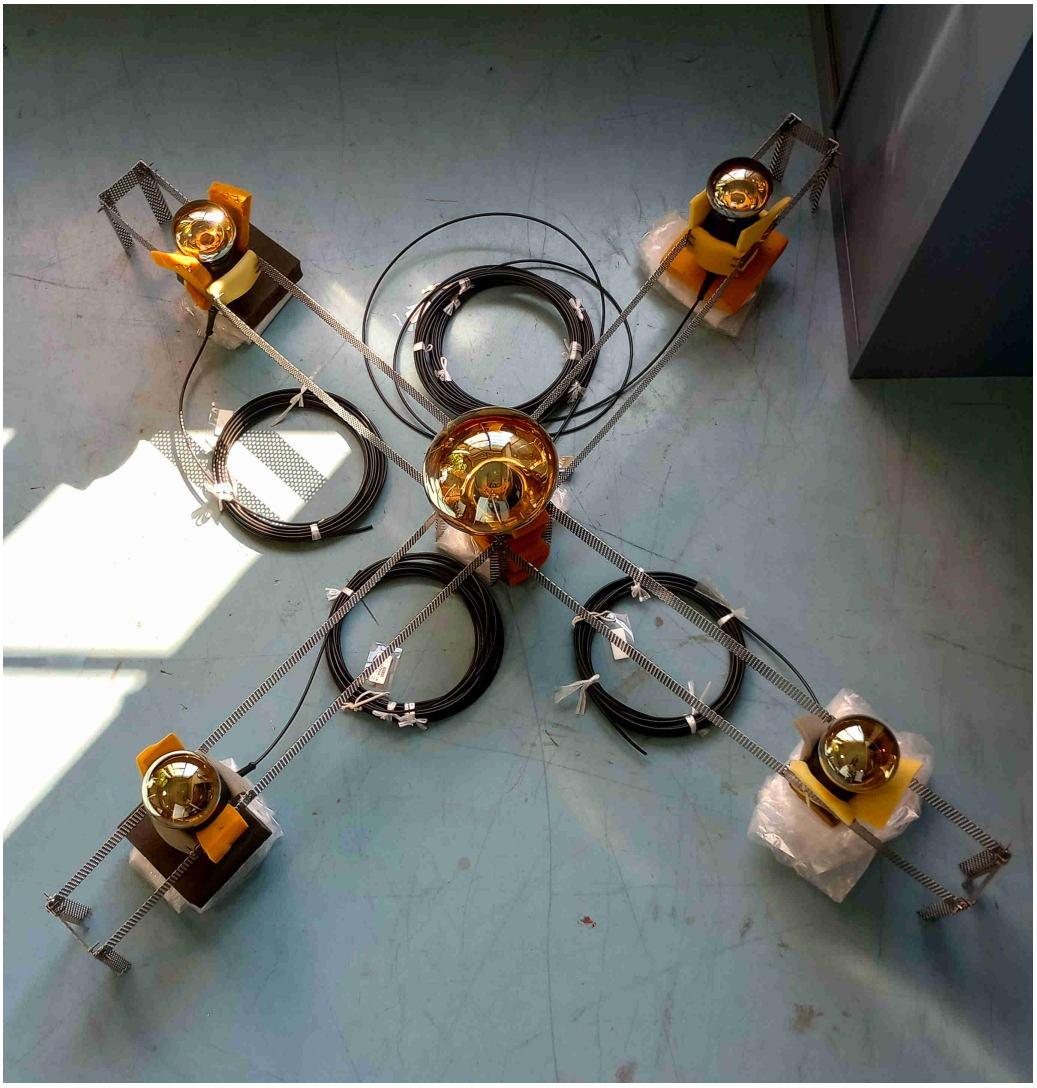

Figure 3.13: Holding test of cross holder using the 5 PMTs of the reference configuration.

The structure has been manually lifted to ensure that the pressure applied by the C-profiles was sufficient to hold the PMTs in place, obtaining positive results. It has been decided however to reinforce the cross arms to limit their flexion during lifting since the structure was very rigid in the vertical direction but not horizontally. It was sufficient to add two C-profiles for each arm to considerably reinforce the cross arms (fig. 3.14).

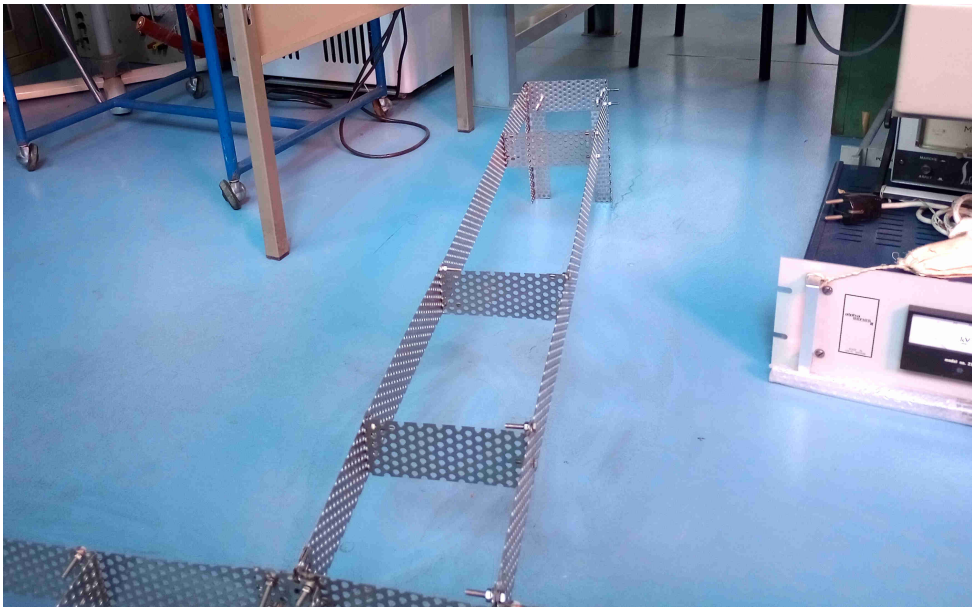

Figure 3.14: Reinforces of the cross arms: 2 additional C-profiles. (One of the two C-profiles used to hold the PMT is not present since it is added only when the PMT is placed.)

4 | Conclusions

4.1. Study on particle detection as a function of the water level

The construction of the prototype tank in the new site is now in progress and it will be completed in the next months. The simulation work on the tank with different water levels in fact, proved that the detection performances improve with a higher water level for muons: detection efficiency increases (linearly), as well as the number of PE detected, while the SD of the first photon time reduces, making particle detection more precise. Results are very similar between 1 GeV and 10 GeV muons, although performances are generally slightly better for the higher energy level. The analysis results led to the change of the installation site from the original one inside a lab to an open-air site able to handle a higher pressure in order to fill the tank up to a higher water level and maximize the detector's capabilities.

The plots reported hereafter sum up the analysis results. Only the scenarios in which the coincidence parameter is considered are shown here for detection efficiency and SD. An additional summary table of all the simulations' results is reported in appendix E.

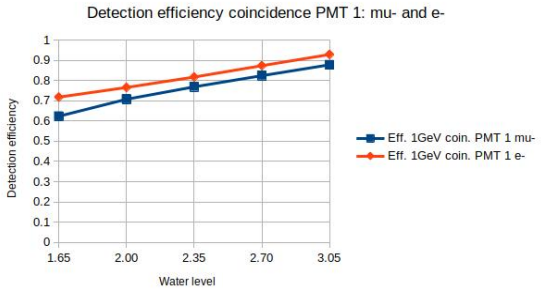

(a) Detection efficiency for the central PMT.

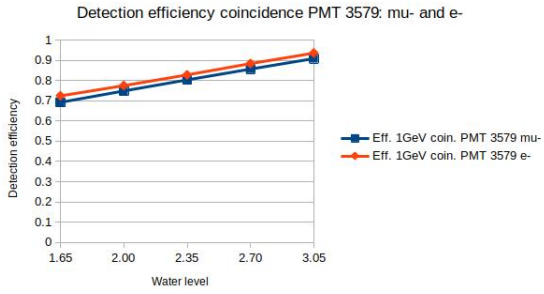

(b) Detection efficiency for the lateral PMTs.

Figure 4.1: Confrontation of detection efficiency (coincidence case) between 1 GeV muons and electrons.

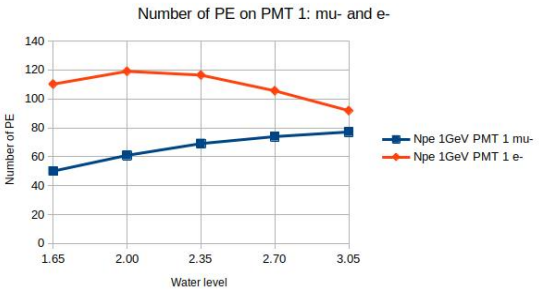

(a) Number of PE detected by the central PMT.

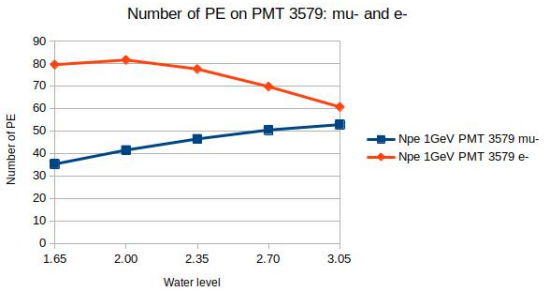

(b) Number of PE detected by the lateral PMTs.

Figure 4.2: Confrontation of the number of PE detected between 1 GeV muons and electrons.

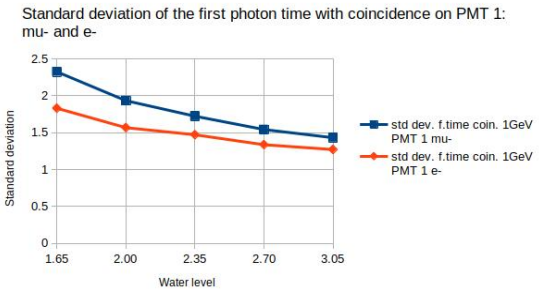

(a) SD of the first photon time on the central PMT.

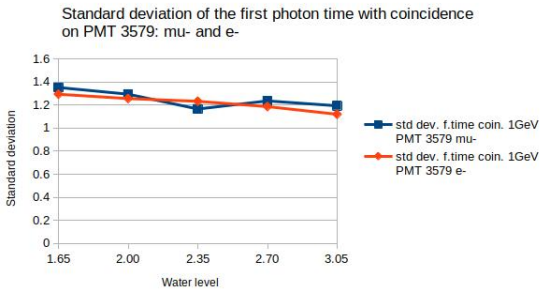

(b) SD of the first photon time on the lateral PMTs.

Figure 4.3: Confrontation of the SD of the first photon time between 1 GeV muons and electrons.

The additional study on electrons, done to verify the model's reliability, showed that, after a certain point, the detection performances reduce with the water level: the detection efficiency increases linearly, but at a lower rate with respect to muons (fig. 4.1), while the number of PE detected starts decreasing after 2.00 m of water height (fig. 4.2); the SD decreases, as for muons, but at a lower rate (fig. 4.3).

4.2. Design of the PMT holder

A big flexible structure able to handle numerous different configurations of PMTs has been designed, but it has been decided to build a smaller one first, that could hold the reference configuration, with which the tests will start as soon as the tank is completed. The structure can be disassembled and its pieces can be recycled for the larger structure when other configurations will be needed.

The installation of the 5 reference configuration PMTs has been tested successfully (fig. 4.4). The structure has also been manually lifted after mounting the PMTs to test its robustness and it has been decided to add two more C-profiles on each arm of the cross as further reinforcement.

Figure 4.4: Test assembly of the PMT holder (before reinforcement of the cross arms).

4.3. Future development

The next step in the prototype tank project development will be the design of the lifting system for the PMT holder. The materials have already been selected but a system of pulleys over the tank will have to be designed, as well as a method to control it precisely from the lab.

The data acquisition from the light sensors will have to be tested too: the PMTs' cables will have to be connected to a station inside the lab, which will have to be equipped for receiving signals from all the types of sensors that will be used.

A procedure to regularly assess the water purity will have to be instituted, but most importantly, a suitable cover for the tank will have to be designed, so that the water is kept clean. The sensors' cables will of course need to pass through it.

After all these steps are concluded and the prototype tank is fully completed and operative, the tests with the reference configuration will start. As soon as the detector is calibrated, it will be ready to be used for testing new types of sensors.

Bibliography

[1] P. Abreu et al. MARTA: a high-energy cosmic-ray detector concept for high-accuracy muon measurement. *The European Physical Journal C*, 78(4):333, Apr. 2018. DOI: https://doi.org/10.1140/epjc/s10052-018-5820-2.

[2] S. Agostinelli et al. GEANT4—a simulation toolkit. *Nuclear Instruments and Methods in Physics Research Section A: Accelerators, Spectrometers, Detectors and Associated Equipment*, 506(3):250–303, Jul. 2003. DOI: https://doi.org/10.1016/S0168-9002(03)01368-8.

[3] F. Aharonian et al. Performance of LHAASO-WCDA and observation of Crab Nebula as a standard candle. arXiv, Jan. 2021. DOI: https://doi.org/10.48550/arXiv.2101.03508.

[4] F. A. Aharonian. LHAASO: A PeVatrons explorer. *Science China Physics, Mechanics Astronomy volume*, 64(10):109531, Aug. 2021. DOI: https://doi.org/10.1007/s11433-021-1751-8.

[5] A. Albert et al. Science case for a wide field-of-view very-high-energy gamma-ray observatory in the Southern hemisphere. arXiv, Feb. 2019. DOI: https://doi.org/10.48550/arXiv.1902.08429.

[6] I. Allekotte et al. The surface detector system of the Pierre Auger observatory. *Nuclear Instruments and Methods in Physics Research Section A: Accelerators, Spectrometers, Detectors and Associated Equipment*, 586(3):409–420, Mar. 2008. DOI: https://doi.org/10.1016/j.nima.2007.12.016.

[7] Azo Materials. Stainless Steel - Grade 304 (UNS S30400). Available at https://www.azom.com/article.aspx?ArticleID=965, Oct. 2001. Online; accessed Nov. 19, 2021.

[8] Azo Materials. Grade 316 stainless steel: Properties, fabrication and applications. Available at https://www.azom.com/article.aspx?ArticleID=2868, May 2005. Online; accessed Nov. 19, 2021.

[9] Bailiff Enterprises. Water, reverse osmosis tank chemical compatibility of common resins, fittings, gaskets and metals. Available at http://doublewalltank.com/chemical2.php?chemical=CHLORINE%20WATER, May 2021. Online; accessed Oct. 16, 2021.

[10] F. Bisconti and A. Chiavassa. Study of water Cherenkov detector design for ground-based gamma-ray experiments. arXiv, May. 2022. DOI: https://doi.org/10.48550/arXiv.2205.02148.

[11] F. Bisconti and A. Chiavassa. Study of water Cherenkov detector designs for the SWGO experiment. *Proceedings of Science*, 395 ICRC2021:895, Mar. 2022. DOI: https://doi.org/10.22323/1.395.0895.

[12] E. Blauffuss. Results from the milagro gamma-ray observatory. *New Astronomy Reviews*, 48(5-6):513–518, Apr. 2004. DOI: https://doi.org/10.1016/j.newar.2003.12.012.

[13] D. Bose and V. Chitnis. Very-high-energy gamma-ray astronomy. *The European Physical Journal Special Topics*, 231(1):1–2, Jan. 2022. DOI: https://doi.org/10.1140/epjs/s11734-022-00444-6.

[14] S. Cecchini and M. Spurio. Atmospheric muons: experimental aspects. *Geoscientific Instrumentation Methods and Data Systems*, 1(2):185–196, Nov. 2012. DOI: https://doi.org/10.5194/gi-1-185-2012.

[15] W. contributors. "milagro (experiment)" in Wikipedia, the free encyclopedia. Available at https://en.wikipedia.org/w/index.php?title=Milagro_(experiment)&oldid=842053766, May 2018. Online; accessed Apr. 10, 2022.

[16] Department of Physics and Astronomy, University of Sheffield. Water Cherenkov detectors. Available at https://www.sheffield.ac.uk/physics/research/particle/neutrino/water-cherenkov, Apr. 2020. Online; accessed Apr. 01, 2022.

[17] A. Etchegoyen et al. Muon-track studies in a water Cherenkov detector. *Nuclear Instruments and Methods in Physics Research Section A: Accelerators, Spectrometers, Detectors and Associated Equipment*, 545(3):602–612, Jun. 2005. DOI: https://doi.org/10.1016/j.nima.2005.02.016.

[18] F. Salesa Greus. Recent results from the HAWC observatory. *Il Nuovo Cimento C*, 40(3):114, Sep. 2017. DOI: https://doi.org/10.1393/ncc/i2017-17114-6.

[19] P. K. F. Grieder. *Cosmic Rays at Earth*. Elsevier, 2001.

[20] HAWC leadership. HAWC: the High-Altitude Water Cherenkov observatory. Available at https://www.hawc-observatory.org/science/. Online; accessed Apr. 08, 2022.

[21] D. Heck et al. CORSIKA: A Monte Carlo code to simulate extensive air showers. *Forschungszentrum Karlsruhe Report FZKA 6019*, 1998. Available at: https://citeseerx.ist.psu.edu/viewdoc/download?doi=10.1.1.531.8061&rep=rep1&type=pdf.

[22] A. M. Hillas. *Cosmic rays*, chapter VI - Extensive Air Showers, pages 83–96. Pergamon. DOI: https://doi.org/10.1016/B978-0-08-016724-4.50009-4.

[23] A. M. Hillas. *TeV Gamma-Ray Astrophysics: Theory and Observations Presented at the Heidelberg Workshop, October 3–7, 1994*, chapter Differences between gamma-ray and hadronic showers, page 17–30. Springer Netherlands, 1996. DOI: https://doi.org/10.1007/978-94-009-0171-1_2.

[24] J. Hinton. The Southern Wide-field Gamma-ray Observatory: status and srospects. *Proceedings of Science*, 395 ICRC2021:023, Mar. 2022. DOI: https://doi.org/10.22323/1.395.0023.

[25] Y. Hu, T. Wang, Y. Mei, Z. Zhang, and C. Ning. A simple setup to measure muon lifetime and electron energy spectrum of muon decay and its Monte Carlo simulation. arXiv, Aug. 2016. DOI: https://doi.org/10.48550/arXiv.1608.06936.

[26] INFN and SWGO collaboration. INFN SWGO letter of intent. 2020.

[27] G. F. Knoll. "radiation measurement - conversion of light to charge" in encyclopedia britannica. Available at https://www.britannica.com/technology/radiation-measurement/Inorganic-scintillators. Online; accessed Mar. 15, 2022.

[28] F. Krennrich. Gamma ray astronomy with atmospheric Cherenkov telescopes: the future. *New Journal of Physics*, 11:115008, Nov. 2009. DOI: https://doi.org/10.1088/1367-2630/11/11/115008.

[29] S. Kunwar. Double-layered water Cherenkov detector for SWGO. *Proceedings of Science*, 395 ICRC2021:902, Mar. 2022. DOI: https://doi.org/10.22323/1.395.0902.

[30] M. de Naurois and D. Mazin. Ground-based detectors in very-high-energy gamma-ray astronomy. *Comptes Rendus Physique*, 16(6-7):610–627, Aug.-Sep. 2015. DOI: https://doi.org/10.1016/j.crhy.2015.08.011.

[31] X. Ma et al. Chapter 1 LHAASO instruments and detector technology. *Chinese Physics C*, 46(3):030001, 2022. DOI: https://doi.org/10.1088/1674-1137/ac3fa6.

[32] M. Mariotti et al. Optimized wavelength shifters light traps with SiPM photo sensors for SWGO. Internal SWGO paper.

[33] D. Martello. Gamma ray observation with EAS. Online: accessed: Ar. 16, 2022, 2010. Available at: https://web2.ba.infn.it/now/now2010/TALKS/sept.9/parallel/Martello.pdf.

[34] F. Montano. Studio delle prestazioni del prototipo del rivelatore Cherenkov ad acqua dell'esperimento SWGO realizzato presso il Politecnico di Milano. Bachelor thesis at Università degli studi di Torino, Sep. 2021.

[35] M. A. Mostafá. The High-Altitude Water Cherenkov observatory. *Brazilian Journal of Physics*, 44(5):571–580, Oct. 2014. DOI: https://doi.org/10.1007/s13538-014-0225-7.

[36] NeoNickel. Hastelloy® alloy. Available at https://www.neonickel.com/it/hastelloy-alloy/. Online; accessed Nov. 06, 2021.

[37] A. Neronov. Introduction to multi-messenger astronomy. *Journal of Physics: Conference Series*, 1263:012001, Jun. 2019. DOI: https://doi.org/10.1088/1742-6596/1263/1/012001.

[38] P. Premovic. Relativistic time dilation and the muon experiment. *The General Science Journal*, Apr. 2020. Available at: https://hal.archives-ouvertes.fr/hal-02531926.

[39] M. C. Reboul and B. Baroux. Metallurgical aspects of corrosion resistance of aluminium alloys. *Materials and Corrosion*, 62(3):215–233, Mar. 2011. DOI: https://doi.org/10.1002/maco.201005650.

[40] G. Reyneke. DI water compatibility chart. Available at https://gregknowswater.com/di-water-compatibility-chart/, Sep. 2010. Online; accessed Oct. 13, 2021.

[41] A. Rimmer. Astronomy enters a new age thanks to multi-messenger signals. Available at: https://astronomy.com/magazine/news/2021/06/the-age-of-multi-messenger--astronomy, Jun. 2021. Online; accessed: May. 1, 2022.

[42] G. Sinnis. The HAWC TeV gamma-ray observatory. *Il nuovo cimento C*, 34(3): 65–70, Jun. 2011. DOI: https://doi.org/10.1393/ncc/i2011-10851-8.

[43] P. Sommers. Extensive air showers and measurement techniques. *Comptes Rendus Physique*, 5(4):463–472, Apr. 2004. DOI: https://doi.org/10.1016/j.crhy.2004.03.009.

[44] C. Spiering. 50 years Institute for Nuclear Research: exploring the high-energy universe. *Physics-Uspekhi*, 64(12):1198, Mar. 2021. DOI: https://doi.org/10.3367/UFNe.2021.06.038998.

[45] P. R. Vormelker and A. J. Duncan. Corrosion evaluation of aluminum alloys in deionized water. Technical report, Westinghouse Savannah River Company, Aiken, South Carolina 29808. Available at: https://sti.srs.gov/fulltext/ms2004654/ms2004654.pdf.

[46] J. Ward, J. Cortina, and D. Guberman. Light-Trap: a SiPM upgrade for VHE astronomy and beyond. *Journal of Instrumentation*, 11, Nov. 2016. DOI: https://doi.org/10.1088/1748-0221/11/11/C11007.

[47] Wikipedia contributors. "high altitude water cherenkov experiment" in Wikipedia, the free encyclopedia. Available at https://en.wikipedia.org/w/index.php?title=High_Altitude_Water_Cherenkov_Experiment&oldid=949625137, Apr. 2020. Online; accessed Apr. 10, 2022.

[48] Wikipedia contributors. "cherenkov radiation" in Wikipedia, the free encyclopedia. Available at https://en.wikipedia.org/w/index.php?title=Cherenkov_radiation&oldid=1079919570, 2022. Online; accessed Apr. 12, 2022.

[49] B. O. Yáñez and A. A. Aguilar-Arevalo. A method to measure the integral vertical intensity and angular distribution of atmospheric muons with a stationary plastic scintillator bar detector. *Nuclear Instruments and Methods in Physics Research Section A: Accelerators, Spectrometers, Detectors and Associated Equipment*, 987(5-6): 164870, Jan. 2021. DOI: https://doi.org/10.1016/j.nima.2020.164870.

A | Simulation and analysis details

A.1. Setting the simulation

To set the simulation parameters, it is necessary to modify HAWCSim simulation files.

First of all, the single tank's dimensions have to be set:

- tank height, in m (3.12)
- tank diameter, in m (3.32)
- water height, in m (changed for each simulation between 1.65, 2.00, 2.35, 2.70 and 3.05)

Secondly, the PMT positions are determined. The software needs the x, y and z coordinates of the PMT's top center point. The data used are reported hereafter in table A.1. The reference frame's origin is in the center of the tank's bottom.

PMTs coordinates

	PMT 1	**PMT 3**	**PMT 5**	**PMT 7**	**PMT 9**
x (unit: cm)	0	83	-83	0	0
y (unit: cm)	0	0	0	83	-83
z (unit: cm)	50	46	46	46	46

Table A.1: Coordinates of the five reference configuration PMTs.

A.2. Particle generation

The particles are generated by the script generateconfig.C, written by Francesca Bisconti, executed in the root environment, by giving it as inputs the shower characteristics. Inputs

of the script:

- Type of particle ("mu-" for muons, "e-" for electrons)
- Number of particles (12000)
- Total moment of the particles in GeV (1 or 10)
- Radius of the circle where particles are randomly generated, in m (1.78)
- Height of the circle where particles are randomly generated, in m (3.22)

The outputs are:

- a .in file, which name contains all the shower's informations given as inputs
- an image containing the plots of the particles' generated characteristics, such as the ones showed in chapter 2, fig. 2.3

A.3. Simulation

The simulation is executed using the .in file as input. The output is a .xcd file, which has to be converted in .root to analyze it.

A.4. Analysis

Every time a simulation is completed, the output is analyzed. The analysis script used is a modified version of Federico Montano's macro used for a similar simulation work.[34]

The main structure of the script is reported as a flux diagram (fig. A.1, fig. A.2, fig. A.3).

The .csv file generated by the script contains the data used to create the plots of detection efficiency, number of PE detected and SD of the first photon time as a function of the water level in libreoffice calc. Every time the analysis script is run, the water level is modified in the simulation files and a new simulation is performed. When the analysis procedure is done on the new simulation output, a new .csv file is not created but a line is added to the already existing one.

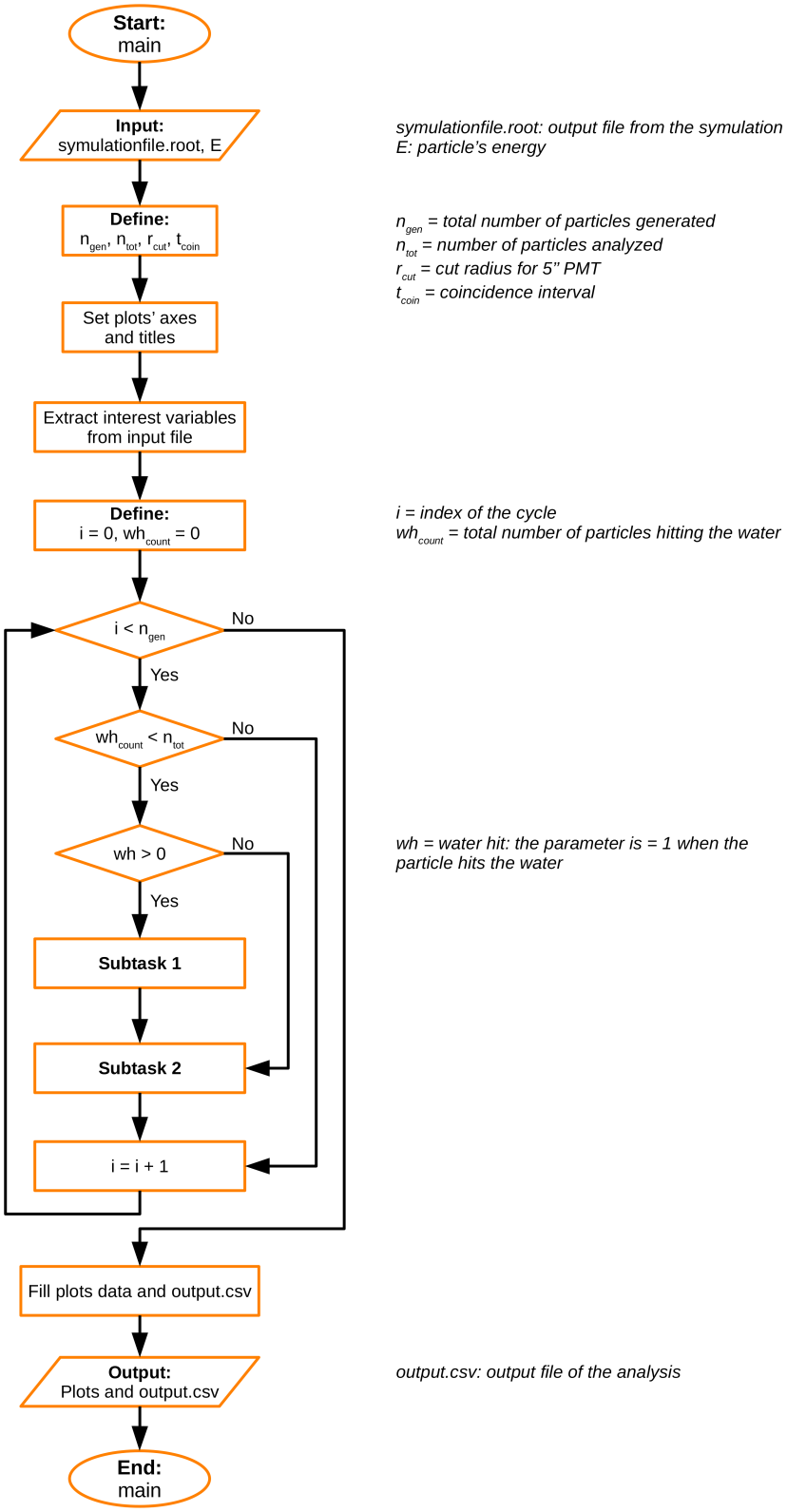

Figure A.1: Flux diagram of the analysis script's main structure.

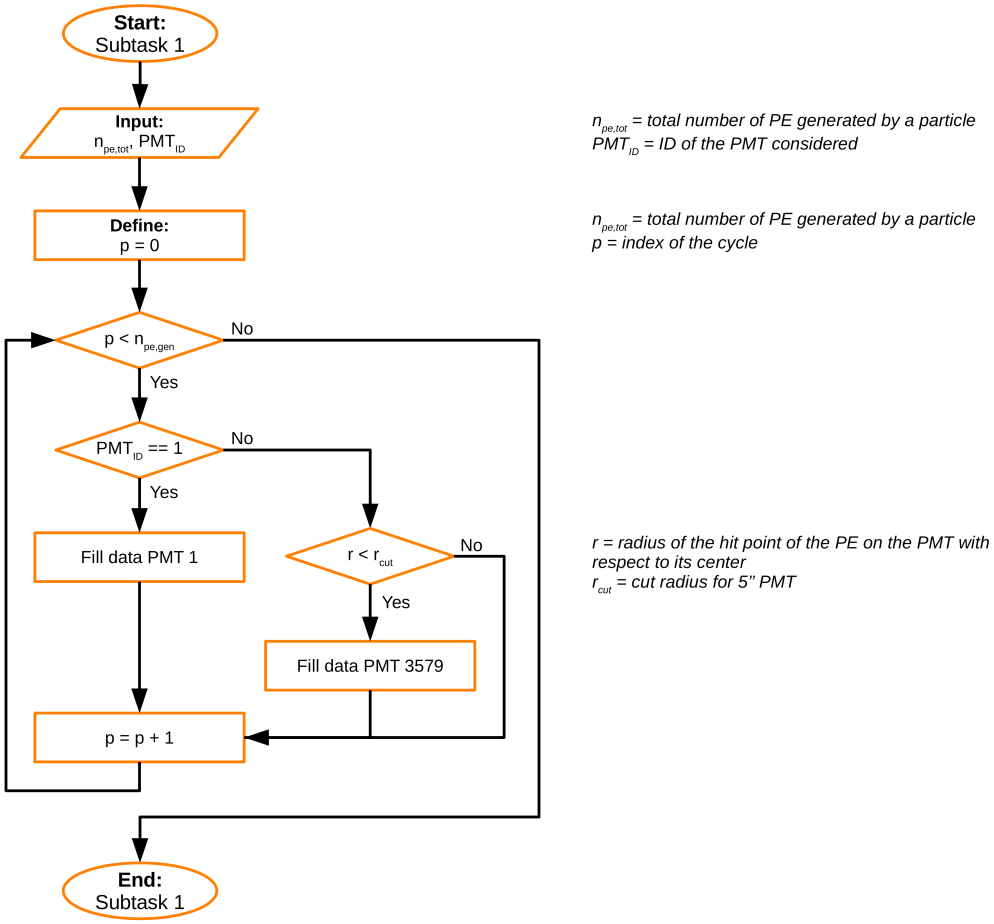

Figure A.2: Flux diagram of Subtask 1's main structure.

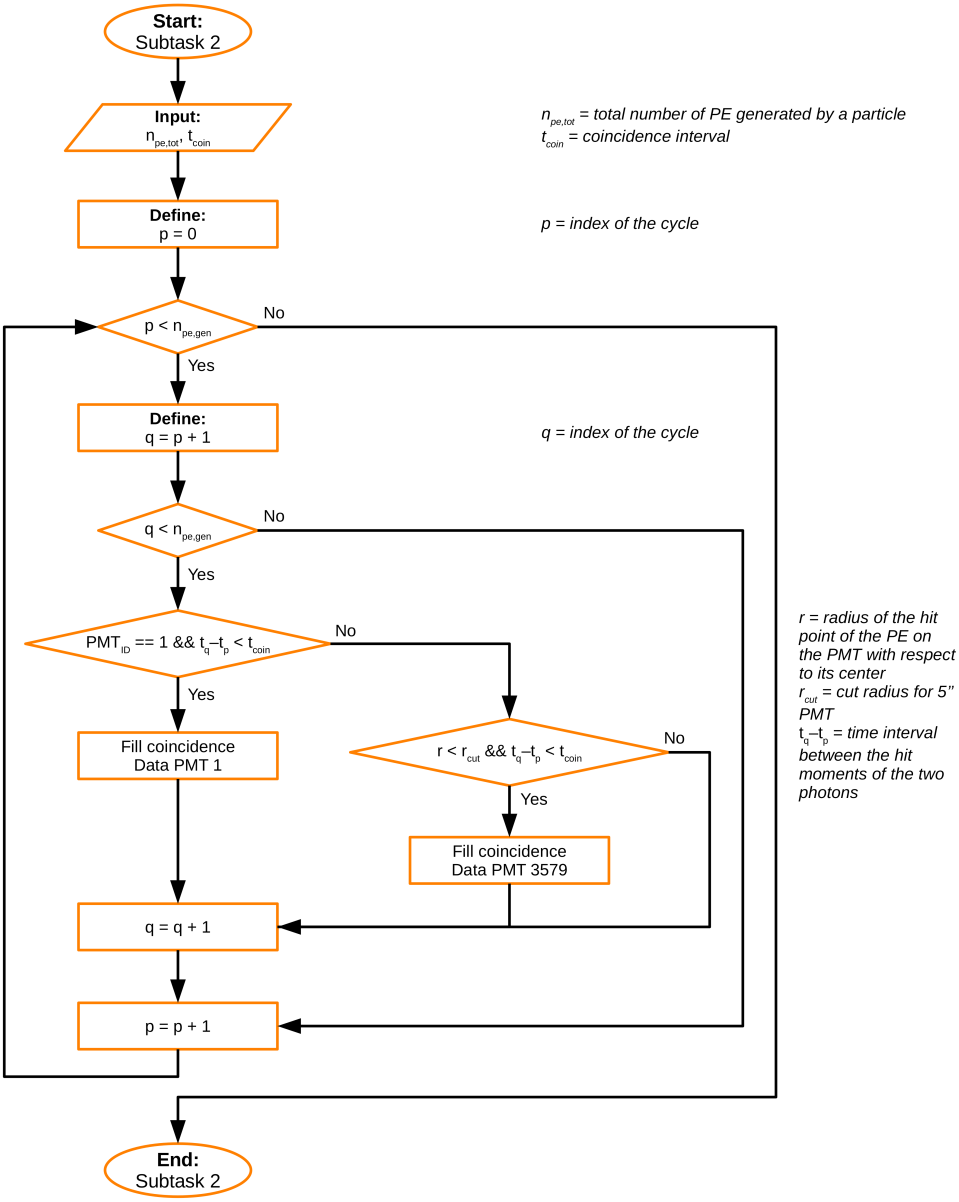

Figure A.3: Flux diagram of Subtask 2's main structure.

B | Materials

List of the materials compatible with purified water assessed for the project [7–9, 36, 40]

Resins/Plastics	Rubbers	Metals
HDPE	Buna-N	Stainless steel AISI 304
EPDM	EPDM	Stainless steel AISI 316
Nylon	Viton	Hastelloy®
PVDF		Aluminum
PVC		
CPVC		
Epoxy		
Hypalon		

Table B.1: Materials compatible with RO water

C | PMTs details

C.1. Hamamatsu: R7081-Y006 (10")

Mass: 2.90 kg

Diameter of the detection area: 253 mm (10")

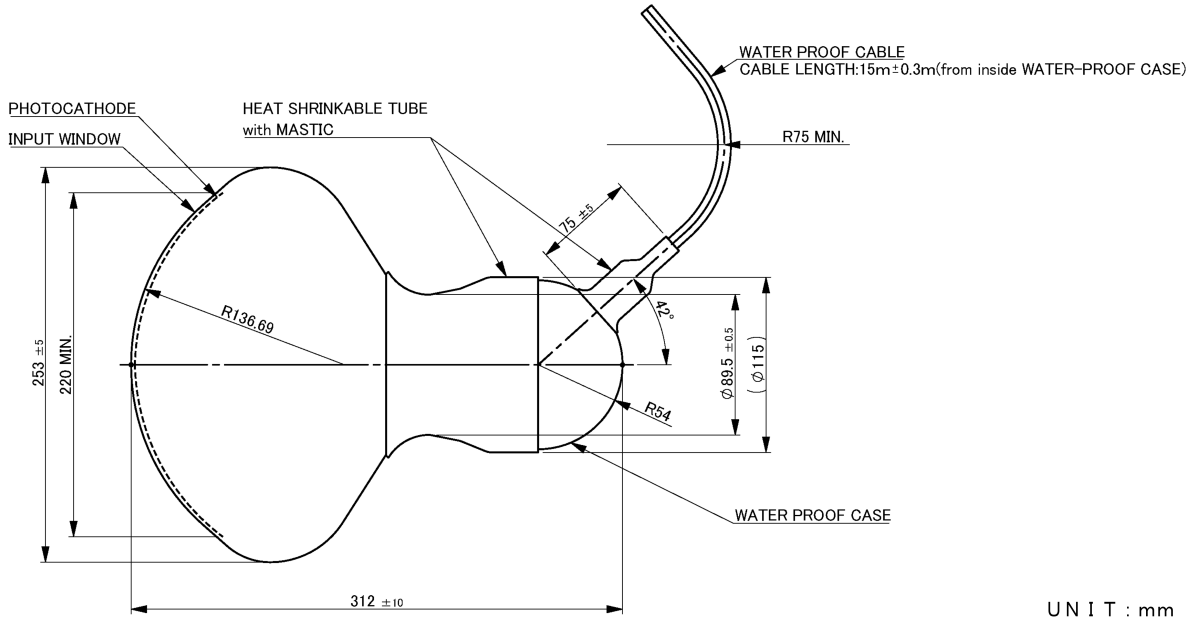

Figure C.1: R7081-Y006 dimensions.

C.2. Hamamatsu: R6594-Y004 (5")

Mass: 2.07 kg

Diameter of the detection area: 128 mm (5")

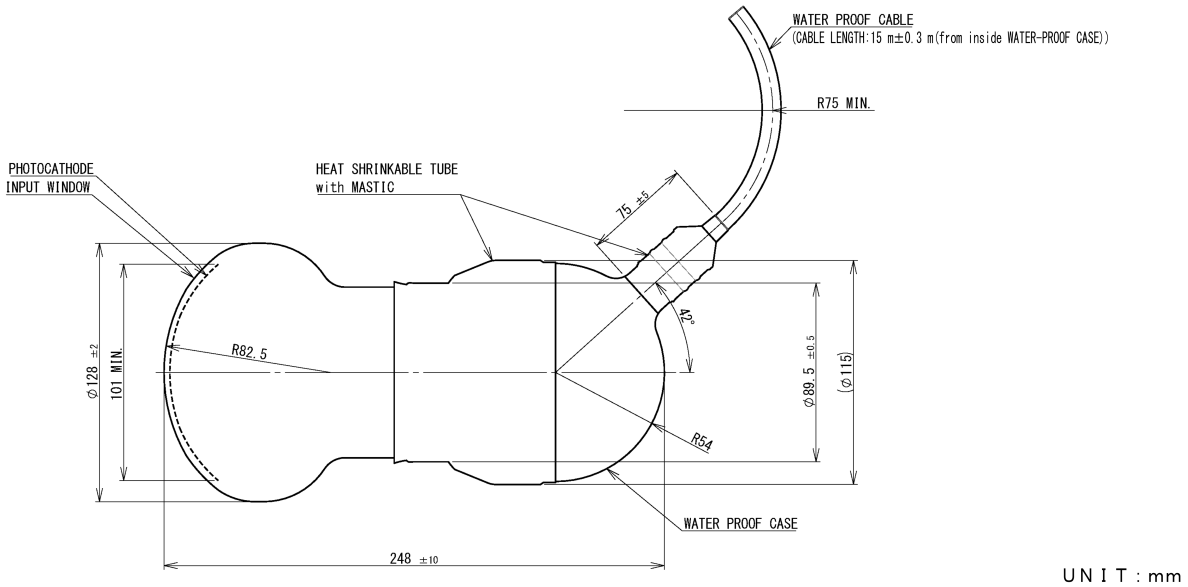

Figure C.2: R6594-Y004 dimensions.

D | PMT holder parts

Technical drawings of the parts manufactured in Politecnico's workshop, used for their cut and folding.

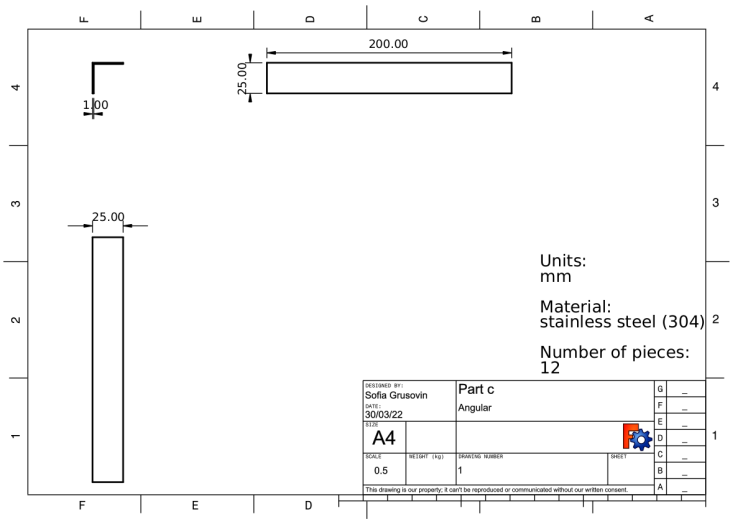

Figure D.1: Part B technical drawing

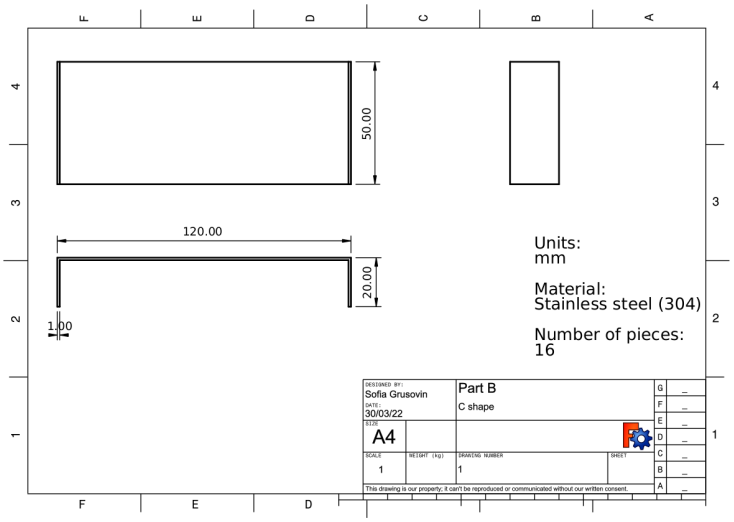

Figure D.2: Part C technical drawing

E | Simulations summary

Summary table of water level analysis

	$\mu-$ 1 GeV	$\mu-$ 10 GeV	$e-$ 1 GeV
eff. PMT 1	+14.49%	+14.02%	+13.48%
eff. PMT 1 coin.	+16.45%	+15.60%	+14.05%
eff. PMT 3579	+13.59%	+13.21%	+13.35%
eff. PMT 3579 coin.	+14.43%	+14.28%	+14.06%
n_{PEscal} **PMT 1**	+21.35%	+25.57%	-11.32%
n_{PEscal} **PMT 3579**	+21.58%	+23.55%	-14.50%
SD PMT 1	-9.99%	-13.71%	-10.54%
SD PMT 1 coin.	-20.20%	-19.01%	-14.72%
SD PMT 3579	-11.60%	-12.38%	-9.94%
SD PMT 3579 coin.	-4.50%	-3.54%	-5.55%

Table E.1: Percentage increase in the analyzed values from the 2.00 m water level scenario to the 2.70 m one.

List of Figures

List of Tables

Nomenclature

EAS	Extensive Air Shower
FoV	Field of View
GC	Galactic Center
HAWC	High Altitude Water Cherenkov gamma-ray observatory
HDPE	High-Eensity PolyEthylene
IACT	Imaging Atmospheric Cherenkov Telescopes
INFN	Istituto Nazionale di Fisica Nucleare
KM2A	Kilometer Square Array
LHAASO	Large High Altitude Air Shower Observatory
PE	PhotoElectron
PMT	PhotoMultiplier Tube
PVC	PolyVinyl Chloride
SD	Standard Deviation
SiPM	Silicon PhotoMultiplier
SWGO	Wide-field Gamma-ray Observatory
UV	UltraViolet
VHE	Very High Energy
WCD	Water Cherenkov Detector
WCDA	Water Cherenkov Detector Array
WFCTA	Wide Field-of-view Cherenkov Telescope Array

List of Symbols

Variable	Description	SI unit
c	speed of light	m/s
$e-$	electron	-
$e+$	positron	-
eff	detection efficiency	-
h	height	m
n	refractive index of a medium	-
n_{part}	number of particles detected by a PMT configuration	-
n_{PE}	number of PE detected by each configuration	-
n_{PEscal}	number of PE detected by each configuration scaled for n_{tot}	-
n_{tot}	total number of particles entering the water	-
r	radius	m
t	time	s
v_p	speed of a particle in a medium	m/s
β	ratio between the speed of the particle and the speed of light	-
γ	gamma ray	-
Θ	emission angle	°
θ	zenith angle	°
$\mu-$	muon	-
$\mu+$	antimuon	-
ϕ	azimuth angle	°

Acknowledgements

I would like to thank all the people from the SWGO collaboration, particularly my advisor professor Giovanni Consolati, doctor Francesca Bisconti, professor Andrea Chiavassa and professor Michele Doro. Many thanks to the people from Politecnico's workshop too, for helping in the construction of the PMT holder. I would also like to thank my family, particularly Luisa, my librarian mother, for her help with the bibliography. Finally, many thanks to all my friends from Politecnico, particularly the Bois, for the mutual support.